Pergamon

Geochimica et Cosmochimica Acta, Vol. 68, No. 22, pp. 4629-4648, 2004

0016-7037/04 $30.00 + .00

doi:10.1016/j.gca.2004.04.024

Rates of silicate dissolution in deep-sea sediment: In situ measurement using $^{234}U/^{238}U$ of pore fluids

KATHARINE MAHER,[1,*] DONALD J. DEPAOLO,[1,2] and JO CHIU-FANG LIN[1]

[1]Department of Earth and Planetary Science, University of California, Berkeley, CA 94720-4767, USA
[2]Earth Sciences Division, E. O. Lawrence Berkeley National Laboratory, 1 Cyclotron Road, Berkeley, CA 94720, USA

(*Received July* 9, 2003; *accepted in revised form April* 12, 2004)

Abstract—Bulk dissolution rates for sediment from ODP Site 984A in the North Atlantic are determined using the $^{234}U/^{238}U$ activity ratios of pore water, bulk sediment, and leachates. Site 984A is one of only several sites where closely spaced pore water samples were obtained from the upper 60 meters of the core; the sedimentation rate is high (11–15 cm/ka), hence the sediments in the upper 60 meters are less than 500 ka old. The sediment is clayey silt and composed mostly of detritus derived from Iceland with a significant component of biogenic carbonate (up to 30%).

The pore water $^{234}U/^{238}U$ activity ratios are higher than seawater values, in the range of 1.2 to 1.6, while the bulk sediment $^{234}U/^{238}U$ activity ratios are close to 1.0. The $^{234}U/^{238}U$ of the pore water reflects a balance between the mineral dissolution rate and the supply rate of excess ^{234}U to the pore fluid by α-recoil injection of ^{234}Th. The fraction of ^{238}U decays that result in α-recoil injection of ^{234}U to pore fluid is estimated to be 0.10 to 0.20 based on the $^{234}U/^{238}U$ of insoluble residue fractions. The calculated bulk dissolution rates, in units of g/g/yr are in the range of 4×10^{-7} to 2×10^{-6} yr^{-1}. There is significant down-hole variability in pore water $^{234}U/^{238}U$ activity ratios (and hence dissolution rates) on a scale of ca. 10 m. The inferred bulk dissolution rate constants are 100 to 10^4 times slower than laboratory-determined rates, 100 times faster than rates inferred for older sediments based on Sr isotopes, and similar to weathering rates determined for terrestrial soils of similar age. The results of this study suggest that U isotopes can be used to measure in situ dissolution rates in fine-grained clastic materials.

The rate estimates for sediments from ODP Site 984 confirm the strong dependence of reactivity on the age of the solid material: the bulk dissolution rate (R_d) of soils and deep-sea sediments can be approximately described by the expression $R_d \approx 0.1\ Age^{-1}$ for ages spanning 1000 to 5×10^8 yr. The age of the material, which encompasses the grain size, surface area, and other chemical factors that contribute to the rate of dissolution, appears to be a much stronger determinant of dissolution rate than any single physical or chemical property of the system.

1. INTRODUCTION

A fundamental objective of geochemistry is to quantify the rates at which minerals and fluids react (Hochella and Banfield, 1995; White and Brantley, 1995; Wood and Walther, 1986). These rates are critical for understanding the role of weathering in climate change (Kump et al., 2000; Lasaga and Berner, 1998), fluid–rock interaction in hydrothermal systems (Wood and Walther, 1983), and reactive chemical transport in a range of contexts from contaminant migration in porous media (Johnson et al., 2000; Luo et al., 2000; Roback et al., 2001) to regional metamorphism (Baxter and DePaolo, 2000). Mineral–fluid reaction rates are also necessary for assessing the degree to which diagenesis modifies the isotopic and chemical records held in sediments (Richter and DePaolo, 1987, 1988; Schrag et al., 1995). The ability to predict natural rates of solid–fluid reactions is limited by the fact that key parameters such as reactive surface area and the free energy departure from equilibrium are difficult to determine in nature (Brantley and Chen, 1995; Brantley and Mellott, 2000; Cama et al., 1999; Hochella and Banfield, 1995; Hodson et al., 1998a, 1998b; Hodson et al., 1997; Jeschke and Dreybrodt, 2002; Lasaga, 1998; White et al., 1996).

The available information for mineral–fluid reaction rates is derived from laboratory experiments (e.g., Blum and Stillings, 1995; Brantley and Chen, 1995; Burch et al., 1993; Chen and Brantley, 1997; Taylor et al., 2000), from studies of soils (Stewart et al., 2001; Taylor and Blum, 1995; White, 1995; White et al., 1996), and from studies of the dissolved loads of streams (Drever, 1988; Drever and Clow, 1995; White et al., 1998). In general, weathering rates (or mineral dissolution rates) in natural environments are significantly slower than the rates measured in laboratory experiments. In addition, estimates of mineral–fluid reaction rates in completely saturated natural systems not in close contact with the atmosphere are few, despite the amount of geochemical research that considers such systems. We describe an approach to determining bulk mineral dissolution and precipitation rates in deep-sea sediments using uranium isotopes in pore fluids and solid phases. This approach follows from analogous studies using Sr isotopes in pore fluids (Richter and DePaolo, 1987, 1988; Schrag et al., 1995). The measurements of solid-phase constituents may also facilitate the radiometric dating of young oceanic sediment.

Deep-sea sediments provide an interesting natural laboratory for studying mineral dissolution and fluid-phase chemistry at low temperature. Numerous studies document the geochemistry and isotopic compositions of U in deep-sea sediments (Anderson, 1982, 1987; Anderson and Fleisher, 1989; Anderson et al., 1989a;

* Author to whom correspondence should be addressed (katem@eps.berkeley.edu).

Anderson et al., 1989c; Barnes and Cochran, 1990; Baskaran et al., 1996; Cochran, 1992; Cochran et al., 1986; Cochran and Krishnaswami, 1980; Colley, 1992; Gariepy et al., 1994; Hillaire-Marcel et al., 1990; Klinkhammer and Palmer, 1991; McKee et al., 1987). In general, the mobility of U during diagenesis is limited because it is relatively insoluble and adsorbs to mineral surfaces. The organic content of the sediment regulates U mobility by affecting the oxidation state of the sediments (Anderson et al., 1989a; Andersson et al., 2001; Barnes and Cochran, 1990; Santschi et al., 1988; Thomson et al., 1990; Zheng et al., 2002a). Pore fluid U concentrations are lowest (ca. 0.5 μg/L or less) in organic carbon-rich sediment, whereas in oxidizing carbonate oozes with low organic content the pore fluid concentrations are only slightly lower than that of seawater, or approximately 3 μg/L. The U concentration of pore fluids is commonly lower than that of seawater, which implies that U is extracted from seawater by either precipitation or adsorption (Anderson et al., 1989b; Barnes and Cochran, 1990; Thomson et al., 1990; Yamada and Tsunogai, 1984). The kinetics of these reactions, along with dissolution, are conveyed by the U isotopic signatures of the fluid and solid phases in the system.

The U isotope system has several advantageous features for measuring dissolution rates. The activity ratio $^{234}U/^{238}U$ involves two nuclides in the same radioactive decay chain. Hence this ratio is just the inverse of the decay constant ratio ($^{234}N/^{238}N = \lambda_{238}/\lambda_{234}$) in an undisturbed, closed system in radioactive equilibrium. Rocks and minerals maintain the equilibrium activity ratio of unity unless they have been disturbed recently by physical or chemical processes such as comminution or leaching; thus unlike other radiogenic isotope systems used in geochemistry, rocks are nearly uniform in $^{234}U/^{238}U$. Fine-grained solids, however, do not quantitatively retain intermediate decay products of uranium because of α-recoil effects (Bonotto and Andrews, 1993; Fleischer, 1980, 1982a, 1988; Kigoshi, 1971; Kronfeld et al., 1975; Ku, 1965). The α-recoil effect causes the $^{234}U/^{238}U$ ratio of fine-grained solids ($<\sim$250 μm in diameter) to depart from the equilibrium value resulting in excess ^{234}U in the interstitial fluid phase. Consequently, fluids in contact with fine-grained rock materials tend to have $^{234}U/^{238}U$ ratios that exceed the equilibrium value, sometimes by more than a factor of 10 (Banner et al., 1990; Hussain and Krishnaswami, 1980; Kaufman et al., 1968; Kronfeld et al., 1975). If the solid phase is dissolving concurrently, the dissolution process supplies U with a low $^{234}U/^{238}U$ ratio to the fluid. Hence, the fluid isotopic composition reflects a balance between the α-recoil effects and the dissolution rate of the solid (Kraemer and Kharaka, 1986; Reynolds et al., 2003; Tricca et al., 2000, 2001).

Given the half-life of ^{234}U (239,000 yr), the U isotope system is also appropriate for dating materials that are less than 500,000 yr old, and hence could be valuable for dating glacial cycles in marine sediments. There has been considerable success in using U and Th to date coral (Cheng et al., 2000; Edwards et al., 1987; Hamelin et al., 1991; Henderson et al., 1993; Stein et al., 1991; Yokoyama and Nguyen, 1980). However, the dating of fine-grained sediments has proven difficult due to postdepositional processes (Delaney and Boyle, 1983; Henderson et al., 2001; Ku, 1965; Slowey et al., 1996). Insight into the behavior of U in Pleistocene sediments could help in further developing methods for sediment dating with U isotopes (Russell et al., 1994).

The isotopic ratio and concentration of U in pore water, bulk sediment, and two selected authigenic fractions of marine sediments are used to evaluate dissolution rates for ODP Site 984A in the North Atlantic. The sediments are unconsolidated and have high porosity (ca. 0.7), so they can be treated as a nearly ideal porous medium (Carter and Raymo, 1999). The sedimentation rates are typically low enough that advection rates are small, and fluid-phase diffusion is the primary means of large-scale chemical transport. Furthermore, the sediments are typically of known age, were deposited systematically and quiescently in a known sequence, and can be treated reasonably well as a one-dimensional system with the ocean as the upper boundary.

2. MATERIAL AND METHODS

2.1. Sample Description and Preparation

The samples analyzed are from the North Atlantic Ocean ODP site 984A (61°25.507′N, 24°04.939′W) drilled during ODP Leg 162. Site 984 is located on the Bjorn Drift on the eastern flank of Reykjanes Ridge (southwest of Iceland) at ~1650 m of water depth (Fig. 1). The sediment has an accumulation rate of approximately 15.4 cm/ka from 0 to 29 m and 11.5 cm/ka from 29 to 97 m depth, and is mainly composed of well-sorted terrigenous silts derived from Iceland (Channell and Lehmen, 1999). The bottom current, which supplies sediment to the drift site, acts to select particles according to their hydraulic dimensions resulting in a condensed grain size distribution. The average grain size, based on relatively few samples that have been measured (Carter and Raymo, 1999), is ~8 μm; ~2/3 of the sediment consists of grains smaller than 20 μm, and only 6% are larger than 63 μm (Fig. 2). The sediments consist of four primary components: biogenic carbonate, plagioclase-rich ice-rafted debris, basaltic material derived from Iceland, and a fine amorphous component that may be biogenic silica (Carter and Raymo, 1999; Wright and Flower, 2002). Foraminiferal abundance and calcium carbonate contents are quite low. Calcium carbonate contents were not measured directly on samples from Hole 984A, but were found to be between 3% and 30%, with an average of 7% in the equivalent depth interval (mcd) of Hole 984 (Fig. 3). The mineralogy of the sediment is dominated by plagioclase, smectite, and quartz, with lesser amounts of illite, kaolinite, and chlorite, in order of decreasing abundance (Carter and Raymo, 1999).

The sediment and pore water samples were collected from 8 to 60 m composite depth (mcd) of Hole 984A. The pore water samples were taken from near the core top down to ~56 mcd. Each sample was extracted from the 144–145-cm interval of each core. Pore water samples were filtered on-ship and measured for major elements, alkalinity, and some trace elements. Some of the chemical properties of the pore fluids are exhibited in Figure 3.

Pore water samples were digested in $HClO_4$ to dissolve any organic material growing in the solution before analysis. This was done to prevent isotopic fractionation between fluid and the in-growth material. Each pore water sample was weighed before digestion. About 3 to 5 drops of concentrated $HClO_4$ was added. The sample was heated on the hotplate for several hours to dryness. After cooling, the residual salt was dissolved in 1N HNO_3 to approximately the volume of the original sample.

The sequential extraction procedure of Tessier et al. (1979), with some modification, was used to attempt to separate the exchangeable and authigenic fractions from the bulk sediment. The exchangeable U was extracted with $MgCl_2$ solution, and the carbonate was extracted using sodium acetate solution. The sediment used in this study has very little organic matter (less than 0.5% (Raymo et al., 1999); therefore, we did not employ a separate leaching procedure to extract U from the organic phase. About 1 g of dry sediment was processed for each sequential extraction. The dried sediment is ground to clay size with agate mortar and pestle and then shaken repeatedly in a glass vial to promote homogeneity. The exchangeable phase is extracted at room temperature by leaching for 1 h with 8 mL of 1M $MgCl_2$ adjusted to

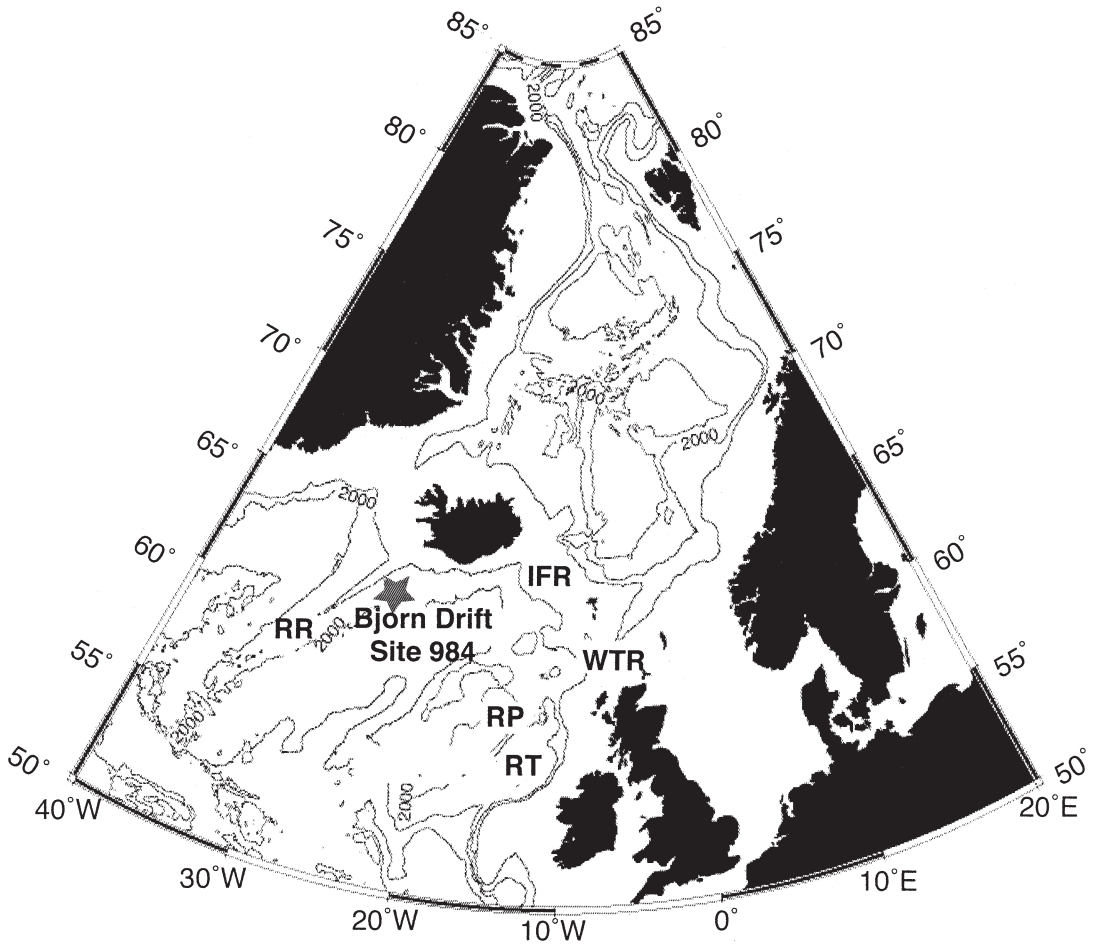

Fig. 1. Location of Site 984 (Bjorn Drift) in the North Atlantic. IFR: Iceland-Faeroe Ridge; WTR: Wyville-Thomson Ridge; RP: Rockall Plateau; RT: Rockall Trough; RR: Reykjanes Ridge.

pH = 7–8 with NH_4OH. The sample is then centrifuged for 20 min, the supernatant weighed and saved for U analysis. The "carbonate" phase is extracted from the residue of the $MgCl_2$ leaching step, using 8 mL of 1M NaOAc adjusted to pH 5 with acetic acid for 5 h. The sample is then centrifuged for 20 min and the supernatant weighed and saved for U analysis. The resulting residues were not analyzed for U isotopes; however, several fresh samples proximal to the original samples were leached in 1.5 N HCl for 30 min in an ultrasonic shaker to remove authigenic phases. After removal of the leachate and subsequent distilled water rinses, the resulting residues were completely digested using concentrated HF-$HClO_4$.

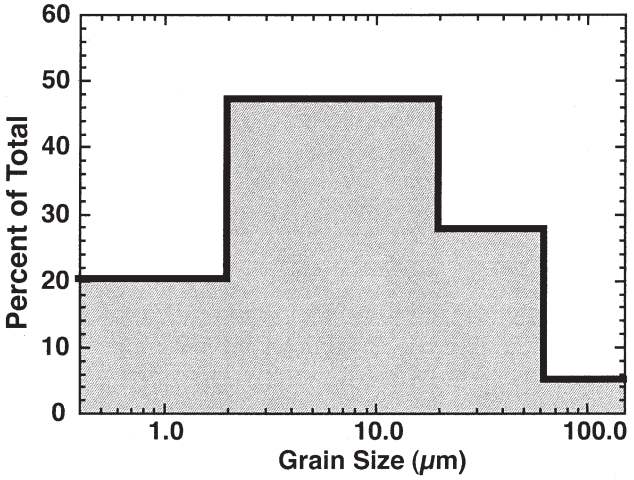

Fig. 2. Grain size distribution for the upper 60 m of Site 984A sediments (from Carter and Raymo, 1999). The mean grain diameter is 5-10 μm.

2.2. Isotope Ratio Measurements

Isotope dilution and isotopic ratio measurements were done on two aliquots of each sample. The concentration measurements were done separately due to the high concentration of the ^{233}U spike at the time of measurements. For the isotope dilution aliquot, ~1 to 10 ng of U was spiked with ^{233}U to a $^{238}U/^{233}U$ ratio of 5 to 10. For the isotopic ratio aliquot in pore waters, the amount of U processed typically was 1 to 3 ng, although in some samples the total was less than 1 ng. For the isotopic ratio aliquot of the sediment and leachates, up to 40 ng of U was processed.

The U was extracted from both sediment and sample solutions using Eichrom UTEVA resin. Approximately 50 μL of UTEVA resin was used for each extraction. After loading the resin onto the column, the column was washed with 60 drops of 0.1N HCl and rinsed with one column-volume of water. The column was then preconditioned with 15 drops of 1N HNO_3. The previously dried sample was dissolved in 5 drops of 1N HNO_3. Sample was centrifuged and loaded onto the column. The column was then washed with 55 drops of 1N HNO_3 and the eluant discarded. The U was then eluted with 50 drops of 0.1 N HCl. Then 1 drop

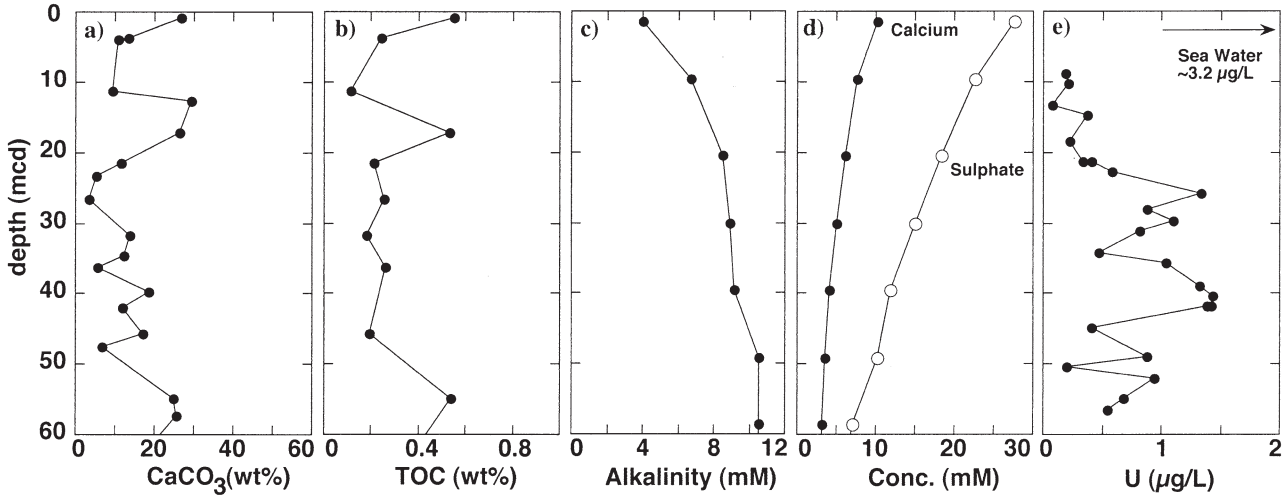

Fig. 3. (a) $CaCO_3$ content, (b) total organic carbon (TOC), (c) pore fluid alkalinity, (d) pore fluid calcium and sulfate concentration, and (e) pore fluid U concentration for Site 984. Data are from Raymo et al. (1999).

of H_3PO_4 and 5 drops of 8 mol/L HNO_3 were added for digesting the organics, and the solution was heated to dryness. The sample was then ready for mass spectrometric measurement.

The strontium of selected pore water samples and NaOAc leachates was extracted and purified using Eichrom Sr-spec resin. About 0.1 mL of each pore fluid and leachate solution was dried for Sr analysis. About 50 μL of Sr-Spec resin was loaded onto small columns custom made with shrinkable Teflon tubing. The columns were first washed with 2 mL of H_2O, then preconditioned with 20 drops of 3N HNO_3. Each sample was dissolved in 2–3 drops of 1N HNO_3 and loaded onto the column. Columns were then washed with 30 drops of 1N HNO_3. Sr was eluted with 1 mL of H_2O. One drop of 0.025M H_3PO_4 was added, and the solution was heated to dryness.

2.3. Mass Spectrometry

Both the isotope dilution and isotopic ratio analyses for all samples except the solid residues were done on a Micromass single collector thermal-ionization mass spectrometer. The instrument is equipped with an analog Daly detector and an axial Faraday cup, with a relative gain of ~100 between the two detectors. Samples were loaded onto single zone-refined Re filaments in 2N HCl graphite colloid solution and H_3PO_4. The $^{234}U/^{238}U$ was calculated from a measurement of $^{234}U/^{235}U$ and assuming the natural abundance ratio of $^{235}U/^{238}U$ to be 1/137.88. The reproducibility of the $^{234}U/^{235}U$ of the U500 standard measured through a 10-month period in 1998 was ~0.1% (2σ) (Table 1). The mean measured value was 0.010425 ± 12, nearly identical to the reported value of 0.0104254. Instrumental mass discrimination was smaller than the external precision of 0.1%. The measurements for the samples, especially the pore fluids, had much larger internal uncertainties than 0.1%, due to the small quantity of U available. Therefore, uncertainties caused by the lack of a fractionation correction are insignificant for this study.

The U isotopic ratios were measured with the mass spectrometer filament temperature between 1750°C and 1900°C. The best ionization efficiency for U (loaded with NIST graphite in ethanol and water) was achieved at filament temperatures between 1800°C and 1850°C. For a sample with 3 ng of U, a ^{235}U beam of ca. 1×10^{-14} Amp can be maintained for 15 to 30 min. This corresponds to an ionization efficiency of ~1.6 to 3×10^{-3}. We found that NIST graphite colloid and ethanol were needed to achieve this level of ionization efficiency.

Five of the pore water samples were measured using a Micromass Isoprobe multi-collector inductively coupled plasma (ICP) mass spectrometer. The $^{234}U/^{238}U$ ratios were measured by comparison with a standard having the secular equilibrium value. Two samples were measured by both thermal ionization mass spectrometry (TIMS) and multi-collector inductively coupled plasma mass spectrometry (MC-ICPMS) for comparison. The agreement between the two measurements was 2–4% of the activity ratio. The precision of the MC-ICPMS measurements was also ±2–4% of the activity ratio. The precision was limited because of small sample size (≤1 ng U). The recently prepared HCl residues were analyzed for $^{234}U/^{238}U$ with the Lawrence Berkeley National Laboratory Isoprobe, and were measured to much higher precision (±0.05% of the activity ratio) as a consequence of larger sample sizes and a procedure that allows for instrumental mass discrimination corrections using the $^{235}U/^{238}U$ ratio (Christensen et al., 2004).

The Sr isotopic ratios were measured using dynamic multi-collection with a TIMS VG Sector 54 instrument. The $^{86}Sr/^{88}Sr$ ratio was normalized to $^{86}Sr/^{88}Sr = 0.1194$, and analyses of the NBS987 Sr standard during the course of this study yielded an average value of 0.71028 ± 2.

3. RESULTS

Figure 3 presents relevant geochemical data for the Site 984A sediments. The organic carbon contents of the sediments are low and show no consistent relationship to the pore water U concentrations. It is generally found that when organic carbon contents are less than 0.5%, U is not likely to be reduced to the +4 oxidation state (Colley et al., 1984; Thomson et al., 1990). Hence it appears that the amount of organic material does not

Table 1. Isotopic measurements of U500 standard.

	Date	$^{234}U/^{235}U$ measured	$^{234}U/^{238}U$ (converted)[a]
U500 65.5 ng U	1/28/98	0.010438 ± 19	0.010435 ± 19
U500 65.5 ng U	2/26/98	0.010393 ± 33	0.010390 ± 33
U500 65.5 ng U	4/8/98	0.010528 ± 18	0.010525 ± 18
U500 65.5 ng U	7/13/98	0.010439 ± 30	0.010436 ± 30
U500 65.5 ng U	8/24/98	0.010423 ± 30	0.010420 ± 30
U500 65.5 ng U	10/9/98	0.010425 ± 28	0.010422 ± 28
U500 65.5 ng U	10/25/98	0.010388 ± 78	0.010385 ± 8
U500 65.5 ng U	11/3/98	0.010395 ± 96	0.010392 ± 10
U500 65.5 ng U	11/11/98	0.010396 ± 17	0.010393 ± 17
average		0.010425 ± 12[b]	0.010422 ± 12[c]

[a] Converted by using the reported $^{235}U/^{238}U$ atomic ratio of 0.999698.

[b] The reported $^{234}U/^{235}U$ value is 0.0104254.

[c] The reported $^{234}U/^{238}U$ value is 0.0104222.

Table 2. U concentration and isotopic ratios of 984A pore fluids.

Sample ID[a]	Depth (mcd)[b]	U (μg/L)	$^{234}U/^{235}U$ measured	$^{234}U/^{238}U$[c] activity ratio
984A 2H-01	8.73	0.187	0.00985 ± 38	1.29 ± 5
984A 2H-02	10.23	0.216	0.00887 ± 27	1.16 ± 4
984A 2H-04	13.23	0.078	0.01179 ± 47	1.54 ± 6
984A 2H-05	14.73	0.370	0.00901 ± 13	1.18 ± 2
984A 3H-01	18.33	0.226	nd	nd
984A 3H-03	21.33	0.329	0.00968 ± 26	1.27 ± 3
984A 3H-03	21.33	0.402	nd	nd
984A 3H-04	22.83	0.580	0.01014 ± 67	1.33 ± 9
984A 3H-06	25.83	1.339	0.01012 ± 16	1.32 ± 2
984A 4H-01	28.14	0.875	nd	1.35 ± 1[d]
984A 4H-02	29.64	1.094	nd	nd
984A 4H-03	31.14	0.817	0.00961 ± 25	1.26 ± 3
984A 4H-05	34.14	0.464	0.00991 ± 19	1.30 ± 2
984A 4H-06	35.64	1.031	0.01217 ± 13	1.59 ± 2
984A 5H-01	38.85	1.318	0.01144 ± 11	1.50 ± 2
984A 5H-02	40.35	1.428	0.01229 ± 13	1.61 ± 2
984A 5H-03	41.85	1.415	0.01177 ± 9	1.54 ± 1
984A 5H-03	41.85	1.386	nd	nd
984A 5H-05	44.85	0.409	0.01107 ± 16	1.45 ± 2
984A 6H-01	48.94	0.881	0.01026 ± 12	1.34 ± 2
984A 6H-02	50.44	0.201	0.01023 ± 42	1.34 ± 5
984A 6H-03	51.94	0.939	nd	nd
984A 6H-05	54.94	0.679	0.01250 ± 15	1.63 ± 2
984A 6H-06	56.44	0.542	0.01033 ± 38	1.35 ± 5

nd = not determined.
[a] All pore waters were taken from 144–145 cm depth of each core.
[b] Meters composite depth for Site 984. The depth is determined by correlating measured properties between different holes to establish a common depth scale for the site (Raymo et al., 1999).
[c] Converted by using the natural $^{235}U/^{238}U$ atomic ratio of 0.007257.
[d] Measured by Micromass IsoProbe.

play a strong role in regulating the pore water U concentration in this core. The decrease in Ca with depth is interpreted as reflecting calcite precipitation associated with sulfate reduction (Raymo et al., 1999).

The U concentration and isotopic ratios of the ODP 162 Hole 984A pore waters are shown in Table 2. Those of the bulk sediment and $MgCl_2$ and NaOAc leachates are listed in Table 3. The U contents of the pore water samples (Fig. 3) are all lower than the seawater value of ~3.2 μg/L, which indicates that remineralization of U from suspended solids in the pore fluids during sampling (and before filtration) was not serious. The pore water concentrations were lowest in the upper 20 meters, with an average value of 0.6 μg/L. U concentrations were somewhat higher but variable in the remainder of the core. The bulk sediment U concentrations are less variable than the pore water concentrations; the average concentration is 1.7 ppm. The low concentration in the bulk sediment for the 13.2 m sample (2H-4) indicates that the sediment at this depth may be dominated by biogenic silica. The shallowest sample has an especially high U concentration. For the cases where bulk sediment and pore fluid U concentration were measured on the same sample, the ratio of bulk sediment–to–pore fluid U concentration varies from 1500 to 7400; the average value for the core is 3500.

The pore water and bulk sediment $^{234}U/^{238}U$ activity ratios are shown in Figure 4. The dashed line in Figure 4 demonstrates how radioactive decay of ^{234}U would cause the $^{234}U/^{238}U$ ratio of pure and unmodified biogenic calcite (i.e., $CaCO_3$ composed only of seawater-derived U) to change with depth. The bulk sediment in the upper meter of the core has a $^{234}U/^{238}U$ ratio that is slightly lower than the seawater value of 1.149 (Chen et al., 1986, Delanghe et al., 2002). Given the high

Table 3. U concentration and isotopic results of 984A bulk sediment and $MgCl_s$ and NaOAc leachates.

Sample ID	Depth (mcd)[a]	Bulk U (μg/g)	Leaching weight loss[b] (%)	Bulk $^{234}U/^{238}U$ activity ratio[c]	Fraction of bulk U in $MgCl_2$ leachate (%)	$^{234}U/^{238}U$ in $MgCl_2$ leachate[c]	Fraction of bulk U in NaOAc leachate (%)	$^{234}U/^{238}U$ in NaOAc leachate[b]	U conc. in NaOAc leachate (ppm)[d]
1H-01 74-75	0.79	2.70	1.37	1.118 ± 10	3.57	1.137 ± 6	17.2	1.125 ± 6	33.6
1H-01 139-140	1.44	1.80		1.095 ± 10	nd	nd	nd	nd	nd
2H-02 139-140	10.23	1.62	2.34	1.014 ± 9	3.67	1.175 ± 13	11.5	1.195 ± 6	7.9
2H-03 139-140	11.73	1.39	0.48	0.957 ± 8	nd	nd	nd	nd	2.0
2H-04 139-140	13.12	0.58	7.33	0.966 ± 25	0.33	1.215 ± 11	1.6	1.348 ± 46	2.0
3H-01 74-75	18.15	1.67[e]	0.45	nd	1.72[e]	1.166 ± 15	9.8[e]	1.168 ± 18	2.2
3H-01 139-140	18.22	1.67	2.33	1.030 ± 9	6.03	1.087 ± 8	13.0	1.102 ± 6	47.3
3H-04 139-140	22.83	1.70		0.959 ± 96	9.62	1.198 ± 17	18.3	1.203 ± 6	13.3
3H-05 139-140	24.33	1.55	1.38	0.973 ± 11	nd	nd	nd	nd	nd
4H-1 139-140	28.14	2.05	6.87	0.979 ± 29	4.28	1.199 ± 9	12.3	1.214 ± 6	18.2
4H-2 74-75	29.46	1.67	1.20	0.964 ± 93	1.01	1.202 ± 29	nd	1.055 ± 211	nd
4H-02 139-140	29.53	2.28	2.73	0.967 ± 31	2.45	1.076 ± 7	6.3	1.076 ± 6	12.0
5H-01 139-140	38.85	1.70		0.979 ± 18	5.88	1.264 ± 20	16.8	1.26 ± 8	10.5
5H-02 139-140	40.24	1.59	2.73	1.002 ± 11	nd	nd	nd	nd	nd
5H-03 139-140	41.85	2.08		0.956 ± 8	2.78	1.307 ± 10	7.6	1.346 ± 11	5.7
5H-05 139-140	44.85	1.95	1.97	1.021 ± 30	nd	nd	nd	nd	nd
6H-5 139-140	54.94	1.19	1.37	1.028 ± 11	2.08	1.616 ± 26	7.0	1.563 ± 66	4.3

nd = not determined due to insufficient sample.
[a] Meters composite depth.
[b] Weight loss after both leaching processes. Corrected for salt content of initial sample.
[c] All activity ratios calculated from measured $^{234}U/^{235}U$ atomic ratios assuming a $^{235}U/^{238}U$ atomic ratio of 0.007257.
[d] Assuming that the weight loss is due to dissolution of the $CaCO_3$ in the sample.
[e] Bulk U concentration for this sample is adopted from the value of 3H-1 139–140. U fraction in $MgCl_2$ and NaOAc leachates were calculated using the adopted bulk U value.

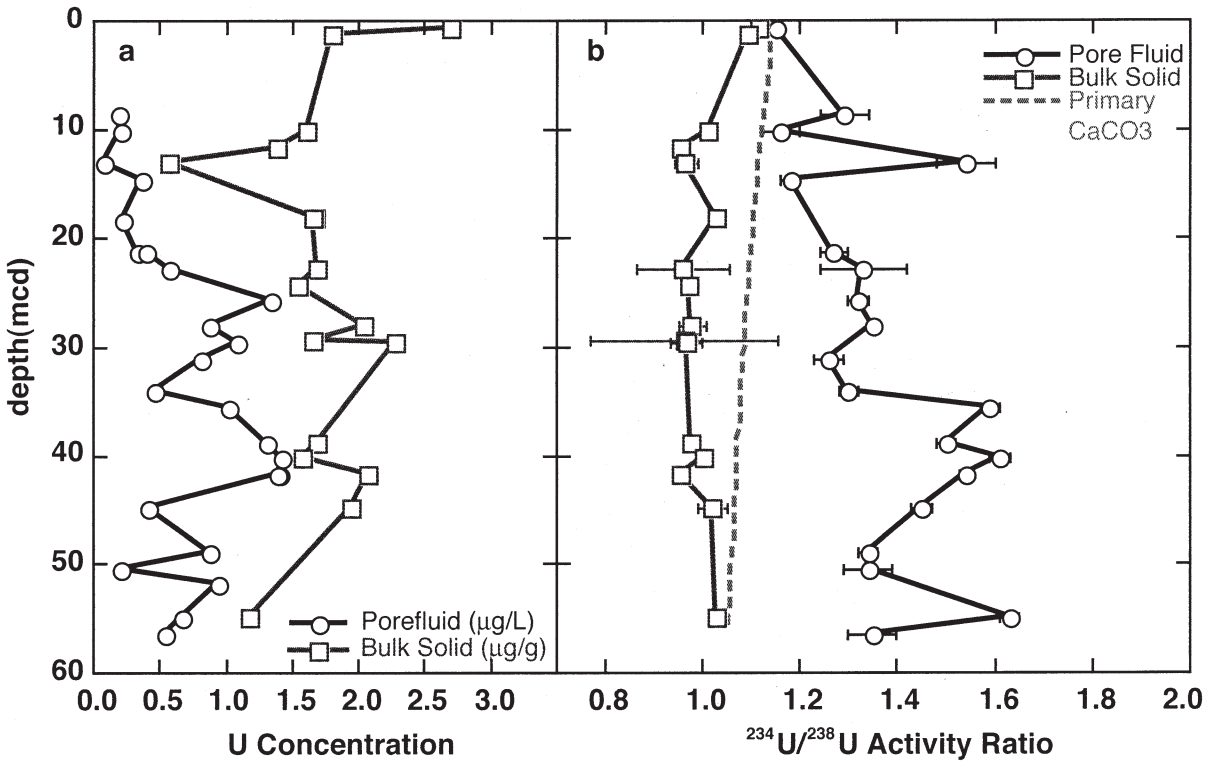

Fig. 4. (a) Pore fluid (μg/L) and bulk solid (μg/g) uranium concentrations for Site 984A. (b) $^{234}U/^{238}U$ activity ratios for pore fluid and bulk solid. Dashed line is the activity ratio that corresponds to the evolution of primary marine calcite formed with the initial seawater $^{234}U/^{238}U$ activity ratio of 1.149.

$CaCO_3$ content in this shallow section of the core, the U budget may be dominated by detrital and/or biogenic calcite and authigenic phases, perhaps as a result of a recent reduction in the terrigenous input. The $^{234}U/^{238}U$ ratios of the remainder of the bulk sediment samples are closer to the secular equilibrium value of 1.0, but there are significant variations between 0.95 and 1.03. As will be discussed further, the bulk values are near unity largely because they are mixtures of detrital material with $^{234}U/^{238}U$ less than or equal to 1.0, and biogenic and authigenic materials with $^{234}U/^{238}U$ higher than 1.0. The pore water $^{234}U/^{238}U$ values are higher than the seawater value and generally increase with depth. The pore water $^{234}U/^{238}U$ values are quite variable on a 10-m scale, and show no significant correlation with U concentration.

The two leaching procedures resulted in the extraction of materials with almost identical $^{234}U/^{238}U$ ratios (Fig. 5). Thus the leachable materials, as expected, appear to consist of a mixture of primary precipitates and authigenic materials derived from the pore water, presumably including adsorbed U. The proportion of authigenic/adsorbed uranium generally increases down-section, but there are large local variations. At 18 and 30 m depth, the uranium in the leachable phase appears to originate almost entirely from primary marine materials. The leachates from the deepest sample (54.95 m depth $\approx$ 340 ka) have $^{234}U/^{238}U$ that is identical to the pore fluid values. In general, it appears that where leaching released relatively small amounts of U in comparison to the $CaCO_3$ contents of the samples (e.g., depths of 13.12 m and 54.95 m) the leachate isotopic composition approaches the pore water value, reflec-

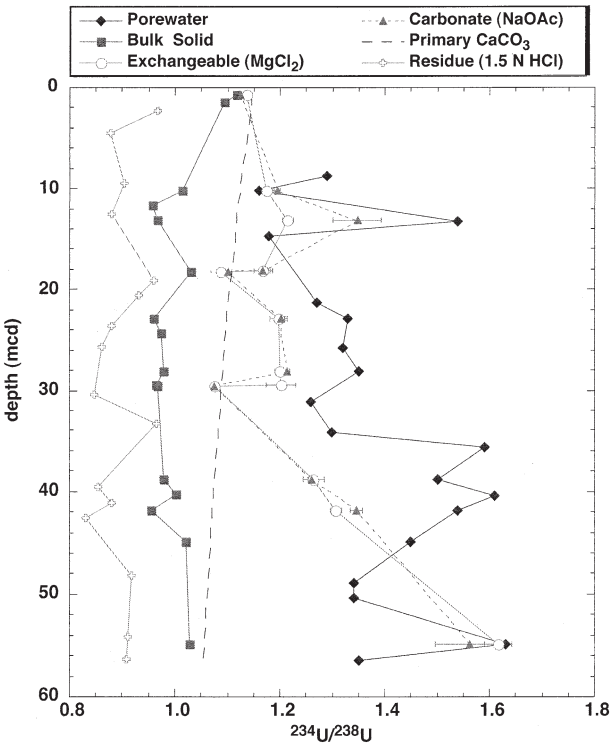

Fig. 5. Measured $^{234}U/^{238}U$ activity ratios in leachates and insoluble residue for the Site 984A samples. Also shown are the data on pore fluid and bulk solid from Figure 4. Dashed line is the activity ratio that corresponds to primary marine calcite formed with the seawater value of 1.149.

Table 4. U activity ratios for primary residues (1.5 N HCl leach).

mcd (m)	$^{234}U/^{238}U$	$\pm 2\ \sigma$
2.30	0.96818	0.00337
4.45	0.87840	0.00200
9.47	0.90398	0.00110
12.48	0.88082	0.00140
19.08	0.96074	0.00191
20.58	0.93208	0.00168
23.58	0.87988	0.00139
25.73	0.86003	0.00137
30.39	0.84774	0.00120
33.39	0.96501	0.00165
39.60	0.85378	0.00140
41.10	0.88016	0.00116
42.60	0.83001	0.00169
48.19	0.91806	0.00150
54.19	0.90960	0.00127
56.34	0.90913	0.00127

tive of greater relative amounts of newly precipitated $CaCO_3$. Where the leaching produced larger U yields (at most other depths) the leachate isotopic composition is closer to the primary marine value, but still shifted substantially toward higher values as a result of the secondary calcite precipitated from the pore water. Hence we conclude that both leach procedures extracted a combination of primary and authigenic U, and therefore do not provide a useful estimate of the isotopic composition of adsorbed U, which should be virtually identical to the pore water values.

The $^{234}U/^{238}U$ activity ratios of the insoluble residues, obtained by leaching separate samples with HCl, are shown in Figure 5. The isotopic values for the residues of the samples below 10 m depth are less than the equilibrium ratio of 1, with an average value of 0.9 and a range of 0.83 to 0.96 (Table 4). The low values are primarily a result of ^{234}U loss from the solid phase as a result of α-recoil ejection of its parent nuclide, ^{234}Th ($t_{1/2}$ = 24.1 d). This effect is commonly observed in fine-grained marine sediments and is discussed in-depth in sections 4.4 and 4.5 (Colley and Thomson, 1992; Hillaire-Marcel et al., 1990; Hussain and Lal, 1986; Ku, 1965; Yamada and Tsunogai, 1984).

The average pore water uranium concentration is ~5 times lower than the value in seawater, and varies from ~2 to 30 times lower than the seawater concentration within the core. This commonly observed uranium concentration reduction in sediment pore fluids has been attributed to either precipitation, adsorption, or both (Klinkhammer and Palmer, 1991). If the reduction were entirely due to adsorption, then the ratio of adsorbed U to dissolved U would be ~5 in the Site 984A sediment. This ratio is not well constrained by the leaching procedures. Both leaching solutions apparently dissolved some solid material that is not in exchange isotopic equilibrium with the pore fluid, because the $^{234}U/^{238}U$ of the leachates is considerably lower than that of the pore fluid in all but one sample (Fig. 5).

The Sr isotopic data (Fig. 6, Table 5) were obtained on pore fluids and NaOAc leachates, but not on the bulk sediment. The pore fluid $^{87}Sr/^{86}Sr$ values vary smoothly and decrease slightly with depth from the seawater value. The

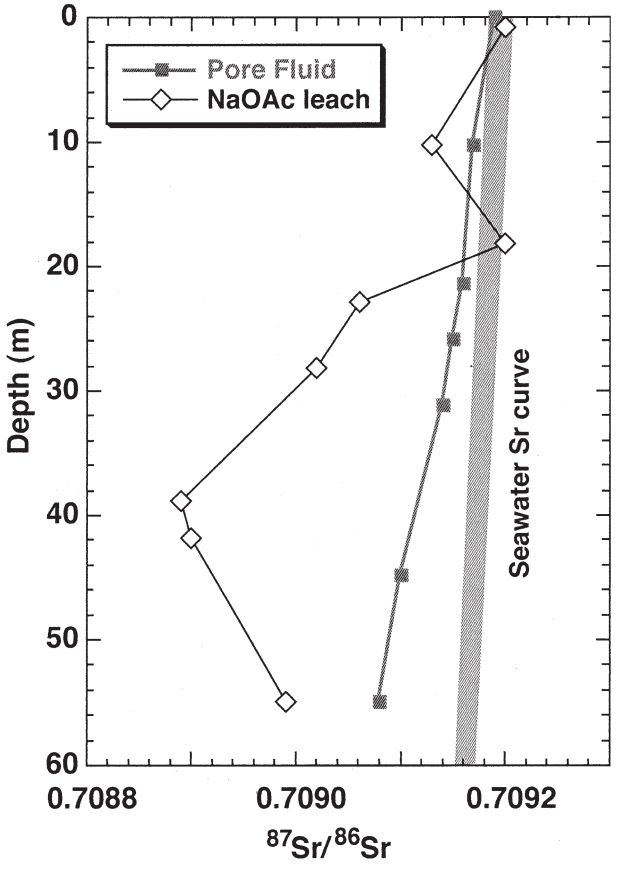

Fig. 6. Sr isotope values for Site 984A for pore fluid and NaOAc leaches. The seawater Sr curve is shown for reference.

Table 5. Sr isotopic ratios of 984A pore fluids and the NaOAc leachate.

Sample ID	Depth (mcd)	Age[a] (ky)	Porewater $^{87}Sr/^{86}Sr$[b]
2H-02 149-150	10.23	66.4	0.70917 ± 1
3H-03 149-150	21.33	138.5	0.70916 ± 1
4H-01 149-150	25.83	167.7	0.70915 ± 1
4H-05 149-150	31.14	270.8	0.70914 ± 1
6H-01 149-150	44.85	390.0	0.70910 ± 1
6H-06 149-150	54.94	477.7	0.70908 ± 1

Sample ID	Depth (mcd)	Age[a] (ky)	NaOAc leachate $^{87}Sr/^{86}Sr$
1H-01 74-75	0.79	5.1	0.70920 ± 1
2H-02 139-140	10.12	65.7	0.70913 ± 1
3H-01 139-140	18.22	118.3	0.70920 ± 1
3H-04 139-140	22.72	147.5	0.70906 ± 1
4H-01 139-140	28.03	182.0	0.70902 ± 1
5H-01 139-140	38.74	336.9	0.70889 ± 1
5H-03 139-140	41.74	363.0	0.70890 ± 1
6H-05 139-140	54.83	476.8	0.70899 ± 1

[a] Ages were calculated using an accumulation rate of 15.4 cm/ka for upper 29 m and 11.5 cm/ka for depths greater than 29 m.

[b] The Sr isotopic ratio was normalized to $^{86}Sr/^{88}Sr$ = 0.1194; The value of the EN-1 standard (Holocene seawater shell) is 0.70919 ± 2.

pore fluid $^{87}Sr/^{86}Sr$ values are expected to decrease with depth due to contributions from the dissolution of both older marine carbonate at greater depth (e.g., Richter and DePaolo, 1987) and the terrigenous volcanic materials that compose the sediment, both of which have lower $^{87}Sr/^{86}Sr$. The NaOAc leaches did not simply dissolve primary marine carbonate, which in the age range represented by this core, changes $^{87}Sr/^{86}Sr$ only slightly relative to the modern seawater value (Capo and DePaolo, 1990; DePaolo and Ingram, 1985; Henderson et al., 1994). The NaOAc leach also did not dissolve only authigenic Sr, because authigenic Sr, having been precipitated from pore water, should have $^{87}Sr/^{86}Sr$ between that of the pore water and modern seawater. The Sr isotopic data indicate that the NaOAc leach attacked silicates, most likely newly formed clays, which may partly account for the fact that the $^{234}U/^{238}U$ values of the NaOAc leachates are lower than those of the corresponding pore water. The smooth variation of $^{87}Sr/^{86}Sr$ with depth in the pore fluid is in marked contrast to the abrupt $^{234}U/^{238}U$ variations. This difference is partly due to the fact that the pore fluid Sr concentration is much higher than that of U relative to the solid-phase concentrations. Hence, diffusive transport of Sr in the pore fluid is effective at smoothing isotopic variations over tens of meters.

4. DISCUSSION

4.1. Interpretive Model

The processes that govern the initial isotopic composition of the sediment are: (i) the deposition of primary carbonate with seawater U activity ratio of 1.149, and (ii) the deposition of primary terrigenous sediment with $^{234}U/^{238}U$ of less than or equal to 1 (according to the age of the parent material, the grain size of the sediment, and its weathering age). Pore water with $^{234}U/^{238}U$ equal to the seawater value is incorporated into sediment at the time of deposition. With time, preferential ejection of ^{234}U from the grains results in enrichment of the pore water in ^{234}U. As the sediment profile ages, there is continuous precipitation of authigenic phases, such as calcium carbonate and amorphous silica (Davis et al., 1987; Richter and Liang, 1993; You et al., 2003). It is assumed that these phases inherit the $^{234}U/^{238}U$ value of the pore water from which they precipitate. Concurrently, dissolution of primary silicate and carbonate phases releases uranium to the pore fluid with a $^{234}U/^{238}U$ value between 0.85 and 1.15. The bulk value of sediment will therefore reflect the "closed" system value, while the U will be partitioned into four components: the insoluble residue, the authigenic fraction, exchangeable fraction, and the pore fluid. The exchangeable fraction is assumed to be in isotopic equilibrium with the pore water. The authigenic fraction at any depth represents an integrated record of pore fluid compositions present at that horizon as the sediment has become buried, modified by any subsequent recoil loss and decay. As the profile ages, the insoluble silicate residue grows more depleted in ^{234}U as a result of continuing recoil loss, and the other phases grow more enriched until steady-state values are reached after several hundred thousand years.

The pore fluid and solid-phase U isotope ratios can be understood with a relatively simple model for the transport of U in solution. The model used here is adapted from those of Johnson and DePaolo (1997), Ku et al. (1992), and Tricca et al. (2000, 2001). An essential characteristic of the system is that the pore fluid contains a small proportion of the U in the sediment-pore fluid system. The U in the pore fluid therefore has a short residence time, and hence the pore fluid isotopic composition mainly reflects local conditions of exchange with the solid phases, rather than vertical transport within the sediment column.

The U transport in solution is reasonably well described with a standard advection-dispersion-exchange formulation:

$$\frac{d(C_f + C_e)(z)}{dt} = D\ \frac{d^2C_f(z)}{dz^2} + (S - v_f)\ \frac{dC_f(z)}{dz} + P(z) \quad (1)$$

where $C_f(z)$ is the concentration of uranium in the fluid phase, C_e is the concentration of adsorbed uranium per unit fluid volume, S is the sedimentation rate, v_f is advective velocity in the vertical direction, and $P(z)$ is the source-sink term for U which includes decay, preferential ejection (in the case of ^{234}U), dissolution, and precipitation. The relative amounts of the dissolved and adsorbed components can be described by a distribution coefficient K_e, which is equal to the ratio of C_e/C_f (Krishnaswami et al., 1982). The retardation factor, R_f can be used to simplify the transport equations:

$$R_f = \left(1 + \frac{C_e}{C_f}\right) = 1 + K_e. \quad (2)$$

C_e can also be expressed as a concentration relative to the amount of solid (C_a), the conversion being described by: $C_e = C_a[\rho s(1-\phi)/\rho f \phi]$. Use of Eqn. 2 in Eqn. 1 assumes that adsorption/desorption is both rapid (instantaneous) and adequately described by a linear isotherm.

The source-sink formulation for dissolved ^{238}U in the fluid is:

$$P(z) = M_s[R_d C_s - R_p K_s C_f] - \lambda C_f(R_f). \quad (3)$$

The first term on the right-hand side of Eqn. 3 represents the dissolution and precipitation rates, and the last term, decay in the dissolved and adsorbed components. All of the concentration terms are in general a function of depth (z). All parameters are defined in Table 6 along with the assumed values.

The source-sink formulation for dissolved ^{234}U in the fluid is:

$$P(z)' = M_s[(f_\alpha \lambda + R_d r_s)C_s - R_p K_s C_f r_f] - \lambda' C_f r_f(R_f') + \lambda C_f(R_f) \quad (4)$$

where the prime is used to distinguish ^{234}U from ^{238}U. The dissolution term in Eqn. 4 is enhanced to include the input of ^{234}U to the pore fluid from alpha recoil of ^{234}Th to the pore water. The f_α parameter, or recoil loss factor is the fraction of ^{238}U decays that result in loss of ^{234}U to the pore fluid; this parameter is discussed in more detail in the subsequent sections.

For the bulk solid (including both the primary material and authigenic phases), the equation for ^{238}U is:

Table 6. Equation parameters and estimated values for Site 984A sediments.

Parameter	Description	Units
A_f	$^{234}U/^{238}U$ activity ratio in pore fluid	
A_s	$^{234}U/^{238}U$ activity ratio in solid phase	
C_a	Concentration of U in adsorbed phase per fluid volume	atoms/vol-fluid
C_f	Concentration of ^{238}U in solution (C' for ^{234}U)	atoms/vol-fluid
C_s	Concentration of U in solid phase	atoms/g-solid
D	Diffusion coefficient of UO_2^{2+} in solution, including tortuosity correction	50 cm^2/yr
ϕ	Porosity	0.7
f_a	Recoil loss factor	0.075–0.17
K_s	Equilibrium distribution coefficient for precipitated solids	C_s/C_f
K_e	Equilibrium distribution coefficient for U adsorption (C_a/C_f)	
k_d	Surface-area normalized dissolution rate constant	mol/m^2/sec
L	Alpha-recoil length	700Å
λ	Decay constant for ^{238}U (λ' for ^{234}U)[a]	yr^{-1}
M_s	Solid mass to fluid unit volume ratio ($\rho_s(1-\phi)/\phi$)	1.0
$P(z)$	Source-sink terms reflecting α-recoil, solid-phase dissolution, precipitation, and exchange with mineral surfaces	atoms/cm^3-total
r_i	$^{234}U/^{238}U$ concentration ratio for phase *i (solid, fluid, etc.)*	
ρ_s, ρ_m	Solid density/Mineral density	2.7 g/cm^3
ρ_f	Fluid density	g/cm^3
R_d	Dissolution rate constant	yr^{-1}
R_p	Precipitation time constant	yr^{-1}
R_f	Retardation factor for U (R_f' for ^{234}U)	
R_s	Mineral dissolution time constant (Surface normalized)	mol/cm^2/s
S	Sedimentation rate	11.5[b]–15[c] cm/ka
SSA	Specific surface area	1.3–3.2 m^2/g
v_f	Fluid velocity relative to the solid phase	cm/ka
z	Depth coordinate in sediment (increasing downward)	m

[a] $\lambda' = 2.83 \times 10^{-6}$ yr^{-1}, $\lambda = 1.55 \times 10^{-10}$ yr^{-1}.
[b] Sedimentation rate for 29 to 97 m is 11.5 cm/ka.
[c] Sedimentation rate for 0 to 29 m is 15.4 cm/ka.

$$\frac{dC_s}{dt} = R_p K_s C_f - (R_d + \lambda) C_s \quad (5)$$

and similarly for ^{234}U:

$$\frac{d\,C_s'}{dt} = R_p K_s C_f' - (R_d + \lambda') C_s' + \lambda(1 - f_\alpha) C_s \quad (6)$$

The assumptions in the above formulations are that: (i) uranium is stoichiometrically released by weathering at the value of the activity ratio of the dissolving solid, which for the present purposes is the activity of the residual solids; (ii) uranium is distributed primarily in the nonquartz minerals (feldspar and clay fractions) and is distributed evenly throughout each grain.

Preferential leaching along damaged recoil tracks has also been proposed as a mechanism of ^{234}U enrichment in natural waters. Extensive laboratory experiments have attempted to quantify the effects of both implantation into neighboring grains (Fleischer, 1980, 1982a,b, 1983; Fleischer and Raabe, 1978), and leaching of ^{234}U from recoil-tracks proximal to the grain surface (Davis and Krogh, 2001; Eyal and Fleischer, 1985; Eyal and Olander, 1990a,b; Hussain and Lal, 1986). Experiments involving implantation of ^{235}U into silicate minerals suggested that up to 70% of the implanted atoms were released within several days of immersion in distilled water (Fleischer, 1982a,b). Given the time scales under consideration here, it is likely that this process has no net effect on the activity ratio of the solid or fluid because the process of decay is slow in comparison to the leaching of implanted daughter products. The intergranular space is quite high for these sediments, thus it is likely that the stopping power of the water will be sufficient to prevent large implantation effects (the recoil range in water is approximately 500Å). Therefore, for the case of implantation followed by release of ^{234}U to solution, any effect from implantation is already considered in the f_α term.

Hussain and Lal (1986) present a model coupled with laboratory data that suggests preferential release of ^{234}U to the fluid along recoil tracks may play a significant role in creating the universally high $^{234}U/^{238}U$ values of natural waters. This effect is subject to several constraints; one is that fresh mineral surfaces must continually be exposed via internal cracks and joints that are made accessible by dissolution of the outer layers. The second is that the contact time between the fluid and solid is short and the weathering rate rapid, such that recoil tracks and "virgin" surfaces are continually exposed. The leaching along recoil tracks is presumably also a function of the age of the material—most laboratory studies documenting preferential release have used very old specimens (i.e., 1.4 Gya monazites; Eyal and Olander, 1990a,b); ages of granites/minerals from Hussain and Lal (1986) and Fleisher (1982a,b, 1983) were not reported). Given the slow weathering rate at Site 984 and the fine grain size (i.e., low internal surface area), preferential leaching is not an important consideration in a model of deep-sea sediments (cf. Hussain and Lal, 1986).

The equations for ^{238}U and ^{234}U can be combined to obtain an expression for the isotope ratio in the fluid and bulk solid phases. This is done using chain rule expressions of the form:

$$C\frac{dr}{dt} = \frac{dC'}{dt} - r\frac{dC}{dt} \tag{7}$$

The resulting expression is then

$$R_f'\frac{\partial r_f}{\partial t} = D\left(\frac{\partial^2 r_f}{\partial z^2}\right) + 2D\frac{R_f'}{R_f}\left(\frac{1}{c_f}\frac{\partial C_f}{\partial z}\frac{\partial r_f}{\partial z}\right) + (S-v)\frac{\partial r_f}{\partial z} + R_d M_s \frac{C_s}{C_f}\left(r_s - \frac{R'}{R}\, r_f\right) + -R_p K_s r_f\left(1 - \frac{R_f'}{R_f}\right) + (\lambda - \lambda')R_f' r_f + \lambda\left(R_f + f_\alpha M_s \frac{C_s}{C_f}\right) \tag{8}$$

If it is assumed that the distribution coefficients are similar for both isotopic species so that $R_f' = R_f$, the resulting equation for the isotope ratio of the fluid is:

$$R_f\frac{\partial r_f}{\partial t} = D\left(\frac{\partial^2 r_f}{\partial z^2} + 2\frac{1}{c_f}\frac{\partial C_f}{\partial z}\frac{\partial r_f}{\partial z}\right) + (S-v)\frac{\partial r_f}{\partial z} + R_d M_s \frac{C_s}{C_f}(r_s - r_f) + (\lambda - \lambda')R_f r_f + \lambda\left(R_f + f_\alpha M_s \frac{C_s}{C_f}\right) \tag{9}$$

The solid isotopic ratio is not affected by dissolution, only by decay and recoil-loss, therefore the evolution of the solid activity ratio is given by:

$$\frac{dr_s}{dt} = R_p K_s \frac{C_f}{C_s}(r_f - r_s) + (\lambda - \lambda')r_s + \lambda(1 - f_\alpha) \tag{10}$$

The pore fluid isotopic ratio can be considered to be at "steady state" ($\partial r_f / \partial_t = 0$) because the time scale for adjustment of the isotopic ratio to the local conditions is short. If the bulk dissolution rate constant is changed, the r_f value adjusts on a time scale of:

$$\tau_{fluid} = \frac{R_f}{R_d M_s \dfrac{C_s}{C_f}} \tag{11}$$

Since the concentration ratio (C_s/C_f) is ~3000 and M_s is on average 1.0, if the bulk dissolution rate constant is $\sim 10^{-6}$ yr^{-1} and (C_e/C_f) is in the range 5 to 10, then the fluid adjustment time is between 2000 and 3700 yr. The fluid adjustment time is short in comparison to the total time for accumulation of the Site 984 sediments (~400 ka). If (C_e/C_f) exceeds ~50, then the steady-state assumption begins to break down.

4.2. Reaction Lengths for U Isotopes

In general, solutions to Eqn. 9 and 10 are required to interpret U isotopic data from fluids and sediment. However, for the Site 984 sediments, the transport terms are small in comparison to the source-sink terms and hence the data can be interpreted adequately by setting the transport terms to zero. This conclusion is reached by consideration of the values of the diffusive and advective reaction lengths that apply to U isotopes, and is essentially a consequence of the large contrast in U concentration between the solids and the fluid.

For a diffusive system, the length scale at which transport in the fluid phase is significant can be estimated from the diffusive reaction length for uranium, Ld_U, defined by:

$$Ld_U = \left(\frac{D}{R_d M_s C_s/C_f}\right)^{1/2} \tag{12}$$

(DePaolo and Getty, 1996). The diffusive reaction length is a measure of the relative magnitudes of the diffusive transport term in comparison to the source-sink terms in Eqns. 1–4. If we substitute the approximate values: $D_{UO}^{2+} = 50$ cm^2/yr (Li and Gregory, 1974; Zheng et al., 2002b), $M_s = 1$, $C_s/C_f = 3000$, and $R_d = 10^{-6}$ yr^{-1}; then we calculate $Ld_U \approx 130$ cm. This result implies that diffusive communication between the ocean and the pore fluid will be confined to a boundary layer extending below the sediment–water interface to a depth of ~4–5 m ($\sim 3Ld_U$), and below that depth the pore fluid is essentially isolated from the ocean for U isotopes. Below the boundary layer, variations of ^{234}U/^{238}U in the pore fluid are smoothed by diffusive transport in the fluid on length scales shorter than 130 cm. On a scale of a few meters, the ^{234}U/^{238}U of the pore fluid behaves as if the sediment and pore fluid are a closed system. The pore fluid isotopic composition therefore reflects mainly the local rates of exchange between the fluid phase and the solid phase, and fluid-phase diffusive transport can be ignored with little loss of accuracy. This analysis is dependent somewhat on the actual value of the dissolution rate. If the dissolution rate constant, R_d, were much smaller than 10^{-6} yr^{-1}, then the diffusive reaction length would be longer. If R_d were 100 times smaller ($LdU \approx 13$ m), diffusion effects would be more significant to the interpretation, especially in the upper half of the core. In the uppermost part of the core, the value of C_s/C_f is greater than 3000 (and as shown below, $R_d > 10^{-6}$ yr^{-1}), so in that region the reaction length is smaller than 3 cm.

The presence of adsorbed U on the solid phase does not affect the calculation of the reaction length because the retardation factor appears in the denominator of both terms in Eqn. 12. Adsorbed U will decrease the value of the ratio C_s/C_f by a factor $1+(C_a/C_f)$, but also decrease the effective diffusivity, D_u, by the same factor. Hence, the value of the reaction length (Eqn. 12) is unaffected by adsorbed U.

The pore fluid also moves slowly by advection, either as a result of lateral or vertical temperature variations, or simply due to compaction of the sediment with depth. The importance of advective transport of dissolved U can be assessed using the advective reaction length for uranium, La_U:

$$La_U = \frac{v_f}{R_d M_s C_s/C_f} \tag{13}$$

The vertical advection velocity of the pore fluid due to compaction is approximately equal to the sedimentation rate (Berner, 1980). At Site 984, the sedimentation rate is ~15.4 cm/ka. Using this value for v_f, the calculated value for La_U is ~8 cm. This means that advecting pore water reequilibrates (with respect to uranium isotopes) to reflect local conditions within ~25 cm distance. Hence, advection also can be ignored in considering the pore fluid isotopic data presented here.

The reaction length that applies to the U concentration in the pore fluid is determined by the rates of adsorption onto and desorption from mineral surfaces. The time scale for adsorption-desorption is short—in the range of hours to days, hence the reaction rate constant for this process is of order 10^2 yr^{-1}, $\sim 10^8$ times faster than the dissolution constant (Braithwaite et al., 2000; Fuhrmann et al., 1997). The reaction length applicable to U concentration in the pore fluid, calculated by substituting 10^2 yr^{-1} for R_d in Eqn. 6, is roughly 0.1 mm. This result indicates that U concentrations in natural waters can be highly variable, even on very short length scales. The pore water data of Barnes and Cochran (1990) clearly show this, as the U concentrations decrease by up to 5 times over distances of 1 to 5 cm below the sediment–water interface in reducing sediments. The data of Figure 3e, and data reported by Tricca et al. (2000, 2001) and many others, confirm that extreme spatial variability in U concentrations is common in natural waters. Uranium concentrations in natural waters are mainly a reflection of local conditions affecting the distribution coefficient that describes the partitioning of U between the adsorbed and the dissolved phases.

4.3. Dissolution Rates in Deep-sea Sediments

4.3.1. Simplified Steady-State Zero-Transport Equations

Given the simplifications discussed above, the equations that describe the uranium isotopic composition of pore fluid and solids as a function of depth below the sediment–water interface are:

$$R_f \frac{\partial A_f}{\partial t} = R_d M_s \frac{C_s}{C_f}(A_s - A_f) + (\lambda - \lambda')R_f A_f + \lambda'\left(R_f + f_\alpha M_s \frac{C_s}{C_f}\right) \quad (14)$$

and for the bulk solids:

$$\frac{dA_s}{dt} = R_p K_s \frac{C_f}{C_s}(A_f - A_s) - \lambda'(A_s - (1 - f_\alpha)) \quad (15)$$

These equations are written in terms of the activity ratio, where $A_i = r_i/r_{eq}$, and $r_{eq} = \lambda/\lambda'$, and incorporate the approximation that $\lambda - \lambda' = -\lambda'$. Equation 14 can be further simplified for the present purposes because the term containing f_α is much larger than R_f. The steady-state equation for the fluid phase is therefore:

$$0 = R_d M_s \frac{C_s}{C_f}(A_s - A_f) + \lambda'(f_\alpha M_s \frac{C_s}{C_f} - A_f R_f) \quad (16)$$

Rearranging Eqn. 16 yields an expression for the isotopic ratio of the fluid:

$$A_f = \frac{R_d A_s + \lambda' f_\alpha}{R_d + R_f \lambda' \frac{C_f}{M_s C_s}} \quad (17)$$

This expression can be simplified because $R_f \lambda' C_f / M_s C_s \ll R_d$, so that the result is (cf. Tricca et al., 2001):

$$A_f = \frac{R_d A_s + \lambda' f_\alpha}{R_d} = A_s + \frac{\lambda' f_\alpha}{R_d} \quad (18)$$

The dissolution rate is therefore simply expressed in terms of the measured activity ratios and the alpha recoil loss factor:

$$R_d = \frac{f_\alpha \lambda'}{A_f - A_s} \quad (19)$$

Equation 19 is the basis for our analysis of the in situ diagenetic reaction rates. The reaction rate is then simply determined by measurements of A_f and A_s, and by the estimate of f_α. The largest uncertainty is likely to be in the estimate of f_α, which we discuss further below. Equation 19 gives an estimate for the dissolution rate that is "instantaneous" and local. It is instantaneous in that it represents an average over a time interval of a few thousand years, which is short in comparison to the age of the sediments, and it is local in that it averages over only a few meters of the sedimentary section.

It is useful to consider also the limiting case of $R_d = 0$, which would correspond to zero solid-phase dissolution. The pore fluid isotopic composition is then determined by preferential injection of ^{234}U due to alpha recoil and the radioactive decay of this ^{234}U in the combined pore fluid and adsorbed components. Using Eqn. 14, the steady-state value of pore fluid activity ratio in the absence of solid-phase dissolution is given by:

$$A_f = 1 + f_\alpha M_s \frac{C_s}{C_f + C_e} \quad (20)$$

Assuming that $C_e/C_f \approx 5$ and $C_s/C_f \approx 3000$, for $f_\alpha = 0.1$ to 0.2 the expected pore fluid activity ratio is $\sim$50 to 100. The fact that the observed values are $\sim$1.4 (Fig. 6) is a clear indication of the substantial effect that solid-phase dissolution has on the pore fluid.

4.3.2. Simplified Solid-Phase Equations

The fluid phase, because it contains such a small proportion of the total U in the system, reaches a (quasi-) steady state rapidly (on a time scale of a few thousand years as given by Eqn. 11), and acquires an isotopic composition that depends on that of the dissolving solid as described by Eqn. 15. The solid-phase activity ratio, however, also changes with time because of both radioactive decay and α-recoil ejection. The time scale for both radioactive decay and alpha recoil ejection is $1/\lambda'$, or $\sim$354 ka, much longer than the time required for the fluid-phase isotopic composition to adjust. Hence, after a few thousand years the fluid-phase isotopic composition reflects the values of A_s, f_α, and the local dissolution rate (R_d), and thereafter the value of A_s evolves on the slower time scale of $1/\lambda'$. When the sediment is old enough, which in practical terms is when the age is greater than about $3/\lambda'$ ($\sim$1 million years), the radioactive decay processes have reached steady state and the isotopic composition of the solid phase no longer changes.

For the Site 984 sediments, the ^{234}U/^{238}U ratio of the *bulk* solid phase evolves because of radioactive decay, α-recoil, and precipitation of secondary minerals. The biogenic carbonate component of the sediment is initially deposited with the seawater value of the ^{234}U/^{238}U activity ratio ($\approx$1.149). With time, this ratio decays to 1.0 if there is no alpha recoil loss, or to $1 -$

f_α if there is recoil loss. Concurrently, the fine-grained silicate particulates, which are deposited with a $^{234}U/^{238}U$ activity ratio ≤ 1.0, are preferentially losing ^{234}U by recoil ejection, and hence their $^{234}U/^{238}U$ activity ratio is evolving toward a steady value of $1 - f_\alpha$. The decay and recoil loss processes cause the $^{234}U/^{238}U$ ratio of the bulk solid to decrease with time. This decrease is offset by the production of authigenic minerals, which form with high $^{234}U/^{238}U$ inherited from the pore fluids.

The simplified equation describing the bulk solid-phase isotopic evolution is derived from Eqn. 15:

$$\frac{dA_s}{dt} \approx R_p K_s \frac{C_f}{C_s} (A_f - A_s) - \lambda'[A_s - (1 - f_\alpha)]. \quad (21)$$

In the absence of precipitation of secondary minerals ($R_p = 0$), the bulk solid-phase activity ratio will decay from its initial value at the time of deposition, to $1 - f_\alpha$ over a period of ~1 Myr. By leaching the sediments with HCl, we expect to remove both primary carbonate and virtually all secondary authigenic components, and thereby recover solid material that behaves according to Eqn. 21 with $R_p = 0$. This material can help us to estimate f_α, and also the initial value of A_s for the noncarbonate fraction.

4.4. Alpha Recoil Injection Factor: Geometric Model

Calculated dissolution rates (Eqn. 19) are proportional to the parameter f_α—the fraction of ^{238}U radioactive decays that result in injection of ^{234}U into the pore fluid due to α-recoil of the ^{234}U progenitor, ^{234}Th ($t_{1/2}$ = 24.1 d). The value of f_α for an individual grain depends on surface to volume ratio of the grain, and the recoil length of the ^{234}Th atom in the grain (Farley, 1996; Kigoshi, 1971). The latter has been estimated at 900 Å or 0.09 μm for zircon (Kigoshi, 1971). When corrected for the difference in mean atomic weight (A_i) and density, using the semiempirical range relationship (Krane, 1988, p. 194):

$$\frac{L_1}{L_2} = \frac{\rho_2}{\rho_1}\left(\frac{A_1}{A_2}\right)^{1/2} \quad (22)$$

the Kigoshi result translates to a recoil length of 0.07 μm for feldspar (ρ = 2700 kg/m^3).

The alpha recoil length is small in comparison to the mean grain size of the Site 984A sediments, which based on the data of Carter and Raymo (1999) is between 5 and 10 μm. Using the model of spherical grains, the expression for f_α is:

$$f_\alpha = \frac{3L}{2d_p} \quad (23)$$

where L is the α-recoil length (μm) and d_p is the diameter of the particle (μm). When applied to natural sediment, the model value for f_α depends not only on the mean grain size, but also on the grain size distribution, which is commonly lognormal in natural sediments. The smaller grain sizes (approximately $\leq$10 μm), despite being a small fraction of the total mass of the sediment, contribute substantially more recoiling ^{234}U per unit mass than larger grains. Thus, the calculated f_α must be summed over all grain size intervals. The f_α value we calculate for the Site 984 sediments, using the published grain size distribution and the spherical grain approximation, is approximately 0.029. Measured surface areas of sediments and soils are typically much larger than geometrical surface areas calculated assuming spherical grains (Hodson, 1998; White, 1995; White et al., 1996). For disk-shaped grains, with a diameter-to-thickness ratio of 10 to 20, which might characterize sheet silicates, the calculated f_α for Site 984 sediments would be increased by a factor of 4 to 7; to values in range 0.12 to 0.20. Brantley and Mellott (2000) propose the following empirical relationship between specific surface area (*SSA*) and mean grain size (d_p) for albite ground in the laboratory:

$$\log SSA = 1.2 - \log d_p \quad (24)$$

where *SSA* is in units of m^2/g and d_p is in units of μm. For d_p = 5 to 10 μm as for Site 984A sediments, the predicted values of *SSA* are 1.6 to 3.2 m^2/g. The f_α value can be calculated from the specific surface area using the relation (Luo et al., 2000):

$$f_\alpha = 0.25(SSA)\rho_m L. \quad (25)$$

Given a mineral density (ρ_m) of 2.7 g/cm^3, L = 0.07 μm, the calculated f_α values for Site 984 sediments are in the range of 0.075 to 0.15.

4.5. Measured Alpha Recoil Ejection Factors

The data obtained on HCl residues can also be used to estimate the f_α values. Sediment grains experience preferential loss of ^{234}U depending on their size, but there is insignificant loss unless the grain diameter is sufficiently small (roughly silt size; particle diameter less than 63 μm). When a small grain is produced by erosion, it begins to preferentially leak ^{234}U to its environment, requiring several mean lives of ^{234}U to reach the steady-state value reflective of its size and fractional loss rate. The $^{234}U/^{238}U$ activity ratio of the bulk grain is a function of time since comminution (i.e., since being reduced to its current size). For grains in sediment with a sedimentation age, t_s, the time since comminution is the sum of the sediment age (t_{sed}) and the time of soil residence plus transport from source area to point of deposition (t_{trans}):

$$A_{meas} = (1 - f_\alpha) + [A_\alpha - (1 - f_\alpha)]e^{-\lambda' t_{trans}} e^{-\lambda' t_{sed}} \quad (26)$$

where A_{meas} is the measured value in the sediment grain. For a sedimentary sequence with known age and a constant grain size distribution, when A_{meas} is plotted against $exp(-\lambda' t_{sed})$, the y intercept gives $1 - f_\alpha$ for the bulk sediment.

Figure 7 shows A_{meas} for the insoluble residues plotted against $exp(-\lambda t_{sed})$. The data plot along two separate trends with nearly identical slopes but different y-intercepts. This is most likely due to variations in the transport time of the sediment before deposition, coupled with slight variations in grain size. The lower trend yields a value of 0.83 for $1 - f_\alpha$, the upper trend a value of 0.89, and initial $^{234}U/^{238}U$ activity ratios (for the zero-age sediment) of 0.89 and 0.96, respectively. Hence the data suggest a bi-modal distribution with f_α values of 0.17 and 0.11. The deduced f_α values are in good agreement with those estimated using the Brantley and Mellott (2000) specific surface area formulation and the recoil length of 0.07 μm (Fig. 8).

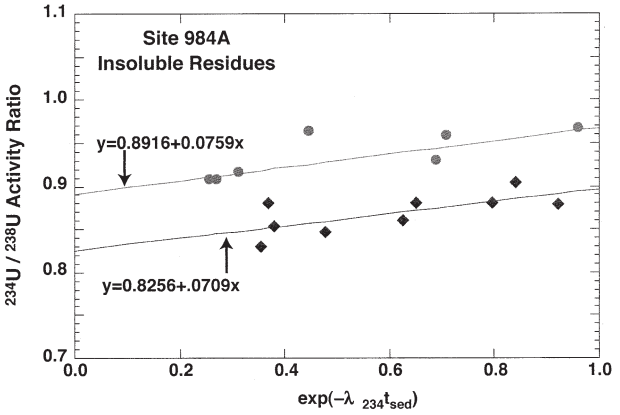

Fig. 7. Measured $^{234}U/^{238}U$ activity ratios for the HCl residues plotted as a function of sedimentation age. Lines represent age corrections showing approximate $^{234}U/^{238}U$ activity ratio upon deposition ($t = 0$), and the value of $1 - f_\alpha$, which can be read at $t = \infty$ or $exp(-\lambda' t_{sed}) = 0$.

4.6. Calculated Bulk Dissolution Rates

Bulk dissolution rates for the Site 984 sediments can be calculated using the estimates of f_α given above (Fig. 8) and the measured activity ratios for the pore fluids and bulk solids. If only the silicate fraction were dissolving, then the residue values could be used instead of the bulk solid values. The calculated dissolution rate constants (R_d values) are in the range 4×10^{-7} to 2×10^{-6} yr^{-1} (Fig. 9a). The R_d values generally decrease from top to bottom in the core from $\geq 10^{-6}$ yr^{-1} at 10 to 15 m depth, to ~4 to 8×10^{-7} yr^{-1} in the bottom third of the core. This decrease in R_d correlates with an increase in sediment age from 60–80 ka to 250–450 ka.

In Figure 9b, the bulk dissolution rate constants are converted to a surface-area normalized mineral dissolution rate constant (k_d, mol/m^2/s) assuming that 50% of the non-$CaCO_3$ fraction is plagioclase with an average molecular weight of 270 g/mol. The rates are plotted as function of depth for a range of f_α values from 0.075 to 0.17 and a range of surface areas.

4.7. Constraints on Rates of $CaCO_3$ Recrystallization

The U isotopic data for the NaOAc leachates reflect a mixture of U contained in primary marine calcite, and U precipitated from the pore water. As the sediment ages, the primary marine calcite is slowly replaced by calcite in isotopic equilibrium with the pore fluid. Because the amount of primary marine calcite deposited initially has varied over time as a function of both climate and the rates of other concurrent diagenetic reactions (i.e., sulfate reduction and anaerobic respiration), it is difficult to quantitatively estimate the rates of recrystallization for calcite based on the U isotopic data alone. However, a simple approximation can be made based on the time scale for complete replacement of the marine calcite by pore water–derived calcite. From Figure 5, the calcite reaches isotopic equilibrium with the pore fluid by a depth of ~56 m, or 480,000 yr. This corresponds to a bulk recrystallization rate of 10^{-6} yr^{-1}, only slightly more rapid than the bulk dissolution rates for the silicate fraction.

4.8. Comparison With Other Estimates of Weathering and Recrystallization Rates

Most of the available data on silicate reaction rates comes from laboratory experiments or studies of soils (Blum and Stillings, 1995; Blum, 1997; Lasaga, 1980; Taylor and Blum, 1995; White and Blum, 1995; White et al., 1996). There are very few data available on weathering rates in groundwater systems, and few estimates for recrystallization rates in deep-sea sediments. Richter and Liang (1993) used Sr isotopic data for pore fluids to estimate the recrystallization rates of deep-sea carbonate sections. A summary of the results is shown as Figure 10, which corresponds to Figure 4 of Richter and Liang (1993). Incorporating pore fluid and solid-phase $^{87}Sr/^{86}Sr$ data into a one-dimensional reactive transport model, they estimated that typical carbonate recrystallization time constants (i.e., solution-precipitation rates) are in the range 10^{-7} to 10^{-8} yr^{-1} for sediments of "zero" age. Most importantly, the rates decrease systematically with age to values of 5×10^{-9} to 5×10^{-10} yr^{-1} for sediments older than ~20 million years.

The calculated dissolution rate constants for the Site 984A sediments, for both bulk sediment and carbonate, are between 2×10^{-6} and 4×10^{-7} yr^{-1}. This range of rates is ~1 order of magnitude higher than the rates inferred from Sr isotopes by Richter and Liang (1993) for sediments of comparable age. This result is surprising because calcite dissolution rates are commonly faster than silicate dissolution rates. The difference between the two results may be due to the lower sensitivity of the Sr isotope approach applied to young sediments with relatively low sedimentation rates. The difference in sensitivity stems from the difference in the size of the reaction length applicable to U isotopes as opposed to Sr isotopes. For Sr, in

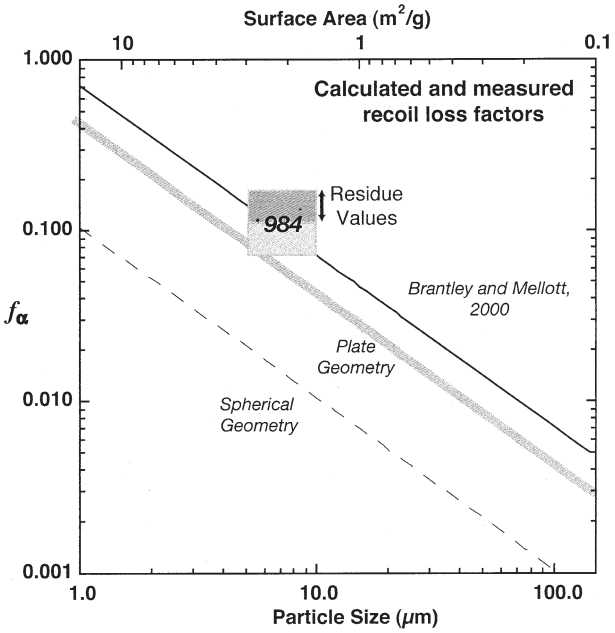

Fig. 8. Calculated and measured alpha recoil loss factors. Dashed line is the spherical model from Eqn. 24, gray line is the model for plate geometry, and black line is the alpha recoil loss calculated from the surface area model of Brantley and Mellott (2000) and Eqn. 25.

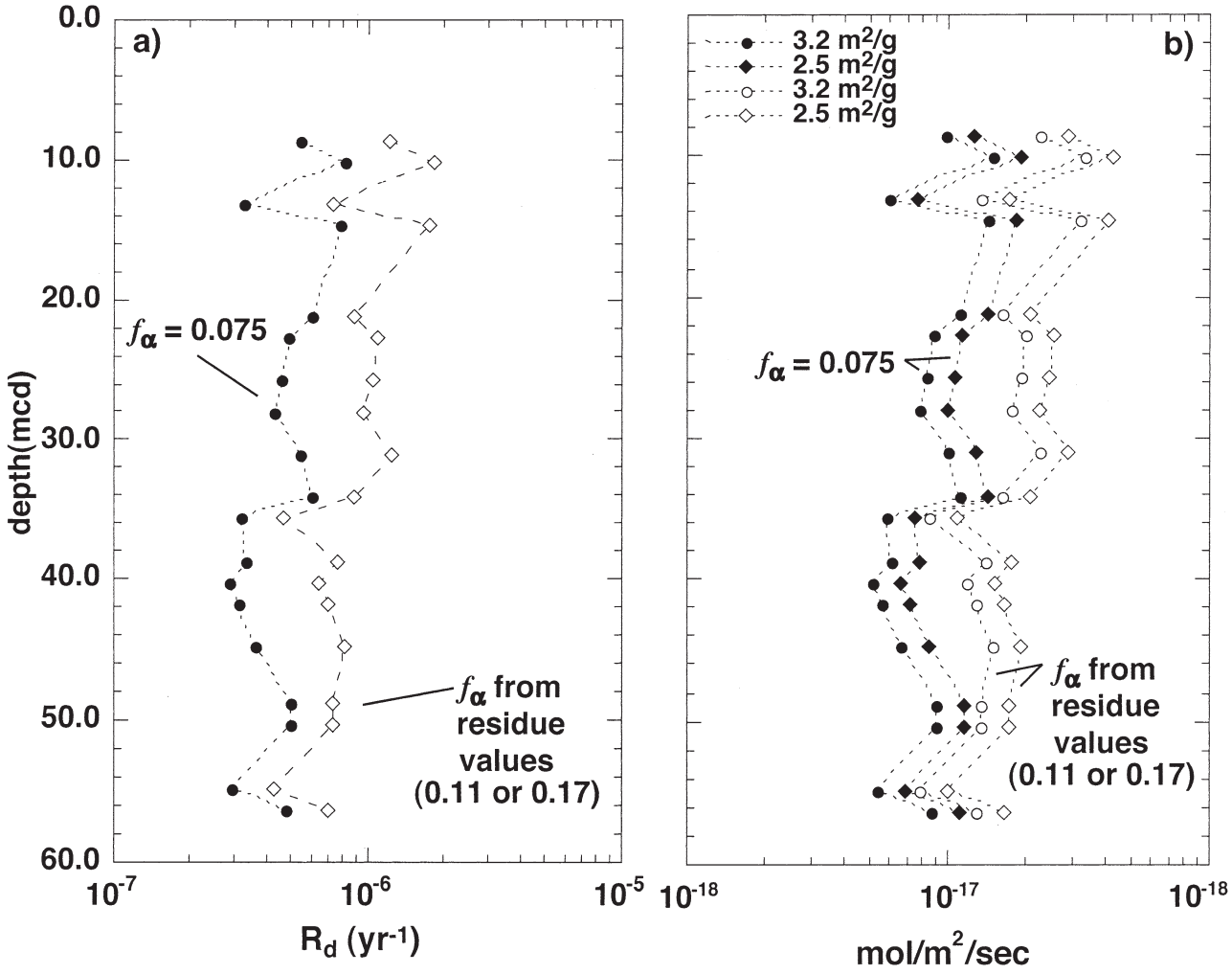

Fig. 9. (a) Calculated dissolution rate constants for 984 sediments as a function of depth. The rates are calculated from Eqn. 19 using the bulk solid values for A_s, for two different assumptions regarding f_α. The curve labeled $f_\alpha = 0.075$ represents the smallest likely value of f_α for the typical average grain size of the Site 984 sediments. The other curve uses the f_α values inferred from Figure 7, and gives our best estimate of the dissolution rate constants. (b) Surface area normalized dissolution rates for Site 984 sediments. These values are calculated assuming that dissolution is dominated by plagioclase, and that 50% of the sediment is plagioclase. The different curves represent different estimates for surface area and the alpha recoil loss factor, f_α. The curves using f_α values inferred from the HCl residue measurements (Fig. 7) are the best estimates. (See text for discussion of surface area calculations).

shallowly buried sediment, C_s/C_f is ~40 (it can vary from 150 to 15), as opposed to C_s/C_f for U, which is almost 10,000 in the upper 20 m of the Site 984A core. The diffusion coefficient for Sr^{2+} is also about twice that for UO_2^{+2} (Li and Gregory, 1974). Consequently, the reaction length for Sr isotopes is ~25 m, which is 20 times larger than the reaction length for U isotopes. This Sr reaction length implies that the fluid-phase Sr isotopic value is an average of the solid–fluid exchange rates over a vertical distance of 75 m or more in the sediment column. The typical sedimentation rate in the carbonate deep-sea cores is ~10–20 m per million years. Hence the Sr isotope signal from sediments in the upper 3 to 6 m of the section, corresponding to ages 0–350 ka, is smoothed by diffusive exchange encompassing the ocean water above and underlying sediments as old as several million years, which have lower recrystallization rates. The peak recrystallization rates applicable to the upper few meters of the sediment column are not accurately reflected in the Sr isotope data. The Site 984A section gives a more accurate characterization of the young sediments both because of the small reaction length for U, and because the sedimentation rate is much higher.

In Figure 11, the Site 984A data are compared to weathering rate estimates from soils (Taylor and Blum, 1995; White, 1995; White et al., 1996), to the laboratory experiments of Davis et al. (1987) regarding the solution-precipitation rate of pure calcium carbonate in a seawater-like solution, and to the review of Blum and Stillings (1995) on the dissolution rate of plagioclase feldspar in water.

The soil data shown in Figure 11 are calculated bulk rates based on individual mineral data, but the bulk rates are very close to the plagioclase feldspar rates. The weathering rates shown involve some assumptions. The raw data consist of the

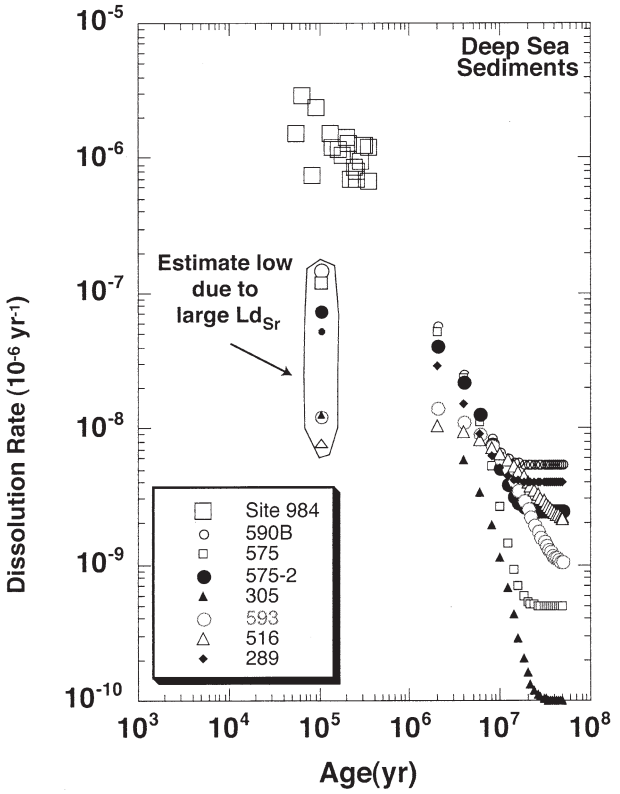

Fig. 10. Comparison of the Site 984A bulk dissolution rate estimates with the dissolution rate (≈ precipitation rate) estimates of Richter and Liang (1993). It is postulated that the discrepancy between the two data sets for ca. 10^5-year-old samples is due to the insensitivity of the Sr system to high dissolution rates confined to the upper few meters of the sediment column.

fraction of the original mineral phase or chemical element remaining in soils of different ages. Given the apparent age dependence of the weathering rates, to estimate the present rate of weathering one must assume a particular mathematical form of the age dependence, then interpret the data in terms of the integrated value of the weathering rate over the life of the soil. We assume the functional form of the weathering rate to be:

$$R(t) = R(t_0)\left(\frac{t_0}{t}\right) \tag{27}$$

where t_0 is a reference age and t is the age of soil. For the White et al. (1996) and White et al. (2001) studies, the reference age is taken to be 130 ka, and for the Taylor and Blum (1995) study the reference age is taken to be 10.9 ka. For the latter, the rates shown for the soils with ages $\leq$10.9 ka are just the average rates over the life of the soils. For soils older than 10.9 ka (and for the soils from the White et al. (1996) study with ages greater than 130 ka), the present-day rates are deduced from the average rates assuming that Eqn. 27 applies.

Figure 11 shows a systematic dependence of weathering rate (dissolution rate or recrystallization rate) on the age of the material, which covers a range in age for natural samples of 5 orders of magnitude, and a range in rates of ~5 to 6 orders of magnitude. The dependence of weathering rate on the age of soils has been noted previously (Hodson and Langan, 1999; Taylor and Blum, 1995; White, 1995; White et al., 1996; White and Brantley, 2003; White et al., 2001). The data plotted in Figure 11 extend the range of ages and rates, and suggest a rather surprising uniformity that includes soils and deep-sea sediments consisting of both carbonate and silicilastic detritus.

The rates displayed in Figure 11 are interesting also because they are constructed using different approaches. The rates determined from soils are based on the volumetric losses of minerals due to dissolution. Although we have converted the data to effective modern in situ rates, the original data represent averages over thousands or even millions of years. For deep-sea sediments, the results of Richter and Liang (1993) are modern in situ values, as are the rates that we calculate with U isotopes. Soils also differ from deep-sea sediments in that soil saturation, temperature, and water chemistry can change daily, seasonally, and because of climate changes, whereas deep-sea sediments are always saturated with seawater-like pore fluid at very slowly varying temperature.

4.9. Implications of Measured Natural Dissolution Rates

Three aspects of Figure 11 are potentially important. One is that the natural rates are in general much lower than laboratory rates, with the exception of the youngest soils. A second is that the rates tend to decrease systematically with age. The third implication is that net dissolution rates for deep-sea sediments never reach zero; even after sediments have been saturated in seawater for tens of millions of years, they are still actively exchanging with the pore fluid. The discussion we provide here is qualitative, but more detailed quantitative analysis of the results is underway.

There has been much discussion in the literature regarding the discrepancies between laboratory and natural rate constants. Blum and Stillings (1995) note that experimental studies typically use freshly ground mineral material, which may have extremely fine grains adhering to the freshly exposed mineral surfaces. With time, the finest grains dissolve away and the surfaces of minerals become armored with secondary precipitates close to equilibrium with the fluid phase. Hochella and Banfield (1995) also present an extended discussion of the mechanisms that may contribute to the general observation that field-based estimates of weathering rates are much lower than laboratory estimates. They mention the density of surface dislocations that promote dissolution, which can change with time and saturation state, the difference between internal surfaces and external surfaces of weathering materials, the properties of water in confined spaces, diffusion limitations in poorly connected void spaces, and others. For sediments, grains with the smallest diameter, and hence the largest surface/volume ratio, dissolve first. The larger average grain size then results in slower reaction (White et al., 1996). Lasaga and Luttge (2001) present a thermodynamic model describing the nonlinear variation in the dissolution rates as equilibrium is approached as a function of the step-wave velocity. The dissolution "stepwave model" quantifies previous observations that reaction rates become highly nonlinear beyond a

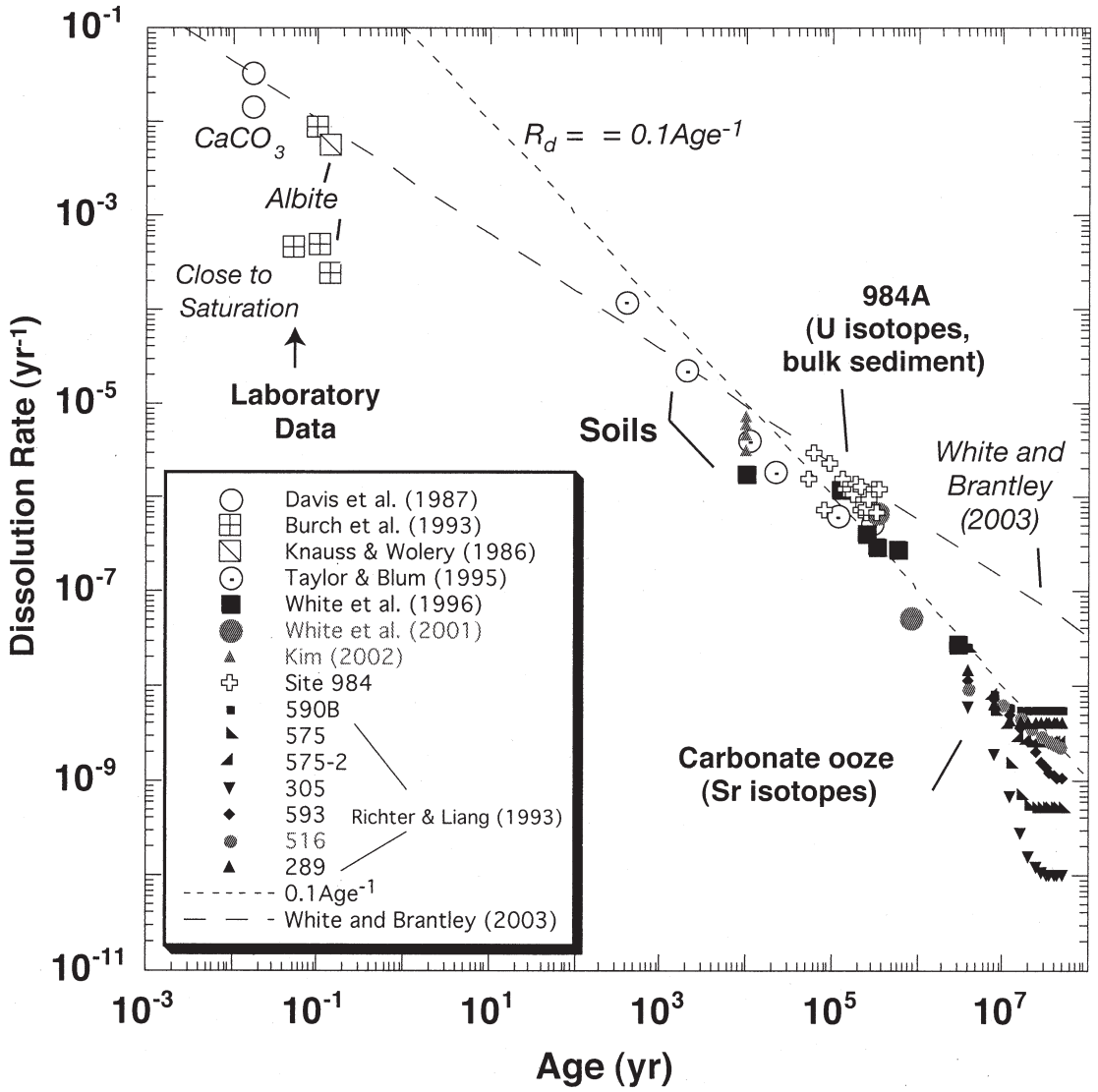

Fig. 11. A broad comparison of dissolution rates for deep-sea sediments from this study and Richter and Liang (1993), weathering rates measured for soil chronosequences (White et al., 1996, 2001; Taylor and Blum, 1995), and laboratory measurements of dissolution rates for carbonate (Davis et al., 1987) and albite (Burch et al., 1993; Knauss and Wolery, 1986). The data from soils are converted using the appropriate parameters as listed in the original study, and the age correction of Eqn. 27 when appropriate (see text). For the White et al. (1996, 2001) and Kim (2002) data, the values were converted using the BET surface areas, and a molecular weight of 270 g/mol. The $CaCO_3$ data are for calcite recrystallization under saturated conditions. The albite dissolution rates measured by Burch et al. (1993) and Knauss and Wolery (1986) are converted to dissolution rates (g/g/yr) using the corresponding BET surface areas and a molecular weight of 270 g/mol. Both data sets are for 25°C. Three of the Burch et al. (1993) samples represent runs conducted at "close to equilibrium" (i.e., $\Delta G_r > -0.5$ kcal/mol); the remainder of the laboratory albite data are within the dissolution rate plateau. Even laboratory studies at close to equilibrium result in higher dissolution rates than natural studies. The "ages" plotted for the experiments represent the approximate duration(s) of the experiments. The dashed line represents the power function determined by White and Brantley (2003), and the dotted line is the best-fit approximation to all natural data ($R_d = 0.1\ Age^{-1}$). The power function given by White and Brantley (2003) is converted to a bulk dissolution rate assuming a surface area of 1 m^2/g and molecular weight of 270 g/mol.

critical undersaturation as a result of the energetics of dislocation defects. These physical and chemical mechanisms provide a thorough rationale for the difference between laboratory and field based estimates of dissolution rates. However, assuming that the soils presented in Figure 11 represent systems close to equilibrium, each of these effects individually can account for differences of only 1 to 2 orders of magnitude in dissolution rate for a specific saturation, and therefore cannot entirely account for the range of observed values.

The empirical age dependence of dissolution rates is potentially useful, insofar as the calculation of reaction rates in natural systems from first principles is fraught with uncertainty. The standard parameterization of reaction rates, in terms of a departure from equilibrium, is determined from the difference between the reaction quotient, Q, and the equilibrium constant, K, modified by

what is normally called the proportion of "reactive surface area," or *RSA* (Lasaga, 1998; Lasaga et al., 1994).

$$Rate = RSA \cdot k_d \cdot \exp\left(\frac{-E_a}{RT}\right)\left(1 - \frac{Q}{K}\right) \qquad (28)$$

RSA is almost impossible to determine precisely, and apparently can differ from the actual surface area by many orders of magnitude (Hodson, 1998; Jeschke and Dreybrodt, 2002; Rufe and Hochella, 1999). As the system approaches equilibrium, it becomes difficult to measure differences between Q and K when the difference is smaller than a few percent of the value. Even at the level of a few percent, the difference is highly uncertain because of issues in determining the activity coefficients (or partial molar free energies) of the reactants—the associated uncertainty in measuring the value of Q is commonly on the order of $\pm 10\%$ at low saturations. For natural systems, kinetic theory is of minimal use in predicting the actual rates of "close-to-equilibrium" natural reactions from measurable thermodynamic parameters. In addition, most of the proposed kinetic theories completely fail to describe the few experiments conducted at low undersaturation (Burch et al., 1993; Nagy et al., 1991). The few experiments conducted at low solution saturation suggest that the predominant mechanism for dissolution changes as the system approaches equilibrium, therefore transition state theory or similar formulations cannot describe dissolution kinetics over the complete range of saturation states of natural systems (Fig. 8, Burch et al., 1993; Lasaga et al., 1994; Nagy and Lasaga, 1992).

Equation 28 predicts that at small undersaturations, the dissolution rate is proportional to $\Delta G_r/RT$. Reaction rates of order 10^{-8} to 10^{-9} yr^{-1} can be produced theoretically by departures from equilibrium in the range of 10^{-3} to 10^{-5} cal/mole. At this level, other energy sources may come into play. A reaction that has a free energy change of 10 kcal/mol that is proceeding at a rate of 10^{-8} to 10^{-9} mol/yr, is using or producing energy at the rate of $\sim 10^{-9}$ to 10^{-10} W/mol. Radioactive decay of U, Th, and K in natural minerals produces about this much energy; which goes into modifying the crystal lattice as well as changing slightly the chemical composition of the mineral. Even if the mineral is nominally at equilibrium with its surroundings, the natural radioactivity is producing chemically unstable domains in minerals at all times. Hence, natural radioactivity could help fuel the continued recrystallization of minerals at the low levels measured for old deep-sea sediments.

The apparently systematic decrease in the dissolution rates with age could have a simple explanation, but the primary determinant remains unknown. It is not unreasonable to propose that soils and sediments should tend to evolve toward a less reactive state. With time, the least stable components should dissolve to be replaced with more stable ones. The surfaces of grains may accumulate coatings that make them less reactive, and the weathering solutions may approach equilibrium with respect to the minerals. In addition, with regard to soils, there may be a trivial limit to the measured rates. If one is measuring reaction rate by the disappearance of a mineral, one cannot measure a rate that is much faster than the reciprocal of the age of the material. Hence it will be a requirement that any dissolution rate measured in this fashion be limited by age. However, there is no requirement that young soils weather faster than old soils, only that old soils must be weathering slowly. In contrast, the measurements of in situ sediment dissolution rates are not limited by age. Carbonate sediments dissolve, but secondary carbonate is precipitated in its place, and the total amount of carbonate changes very little. This is also the case with silicate sediments.

Figure 11 suggests that in a variety of natural circumstances the dissolution rate is mainly a function of the age of the material that is dissolving. Age in this context is the time since the beginning of soil development, or the time since sediment deposition. The typical value for the reaction rate is approximately $R_d \approx 0.1Age^{-1}$. Deviations from this value of up to a factor of 10 may characterize individual major minerals, as suggested by the soil data of White et al. (1996). Nevertheless, this empirical "law" may provide a good approximation to the natural rates, and is likely to be much more accurate than an estimate based on kinetic theory. The empirical relation also requires much less characterization of the natural materials to arrive at a rate estimate.

5. CONCLUSIONS

The results from this study demonstrate that U isotopes in pore fluid can be useful for estimating the in situ (and geologically "instantaneous") dissolution rates of silicates and carbonates. The advantages of U isotopes for estimating dissolution rates are that the solid phase tends to have a $^{234}U/^{238}U$ activity ratio close to unity independent of lithology, and that the low concentration of U in most natural waters results in a small value of the U isotopic reaction length and hence high spatial resolution. Both the average value and the spatial variability of dissolution rates can be evaluated with U isotope studies.

The results from this study provide a link between the dissolution rate estimates based on Sr isotopes in deep-sea carbonate sections (Richter and DePaolo, 1987, 1988; Richter and Liang, 1993) and those determined for soil chronosequences (Taylor and Blum, 1995; White et al., 1996; White et al., 2001). The existing data now show clearly that there is a strong dependence of weathering rate or dissolution rate on the "age" of the material being weathered, where "age" corresponds to the length of time the material has been in the weathering environment. Although age dependence has been noted previously, and various models for its origin have been advanced, it is not clear that any of the proposed models can account for the observed range in rates of a factor of 10^7 or 10^8 (Fig. 11). The age–dissolution rate correlation holds for deep-sea sediments that are saturated and not exposed to air, as well as for soils that are typically unsaturated and exposed to air.

The available data on the natural mineral dissolution rates in natural waters at earth surface conditions, and with close-to-neutral pH, suggest that the dissolution rate will be close to $0.1Age^{-1}$. The dependence on solution chemistry and mineral chemistry appears to be secondary, and to first-order unimportant. This result requires further validation, but may be useful for many types of reactive transport modeling of natural systems where order-of-magnitude estimates of rates are needed, and it is difficult to accurately predict dissolution rates from theory. The results also indicate that sediments and their pore waters continue to react indefinitely ($>10^8$ yr) at slow but nonzero rates.

Acknowledgments—This research was supported by the Director, Office of Science, Basic Energy Sciences, Chemical Sciences, Biosciences and Geosciences Division of the U.S. Department of Energy under Contract No. De-AC03-76SF00098.

Associate editor: S. Krishnaswami

REFERENCES

Anderson R. F. (1982) Concentration, vertical flux, and remineralization of particulate uranium in sea-water. *Geochim. Cosmochim. Acta* **46,** 1293–1299.

Anderson R. F. (1987) Redox behavior of uranium in an anoxic marine basin. *Uranium* **3,** 145–164.

Anderson R. F,. and Fleisher M. Q. (1989) Uranium precipitation in Black Sea sediments. *NATO Advanced Study Institutes Series. Series C; Mathematical and Physical Sciences.* **351,** 443–458.

Anderson R. F., Fleisher M. Q., and LeHuray A. P. (1989a) Concentration, oxidation state, and particulate flux of uranium in the Black Sea. *Geochim. Cosmochim. Acta* **53,** 2215–2224.

Anderson R. F., Fleisher M. Q., and Lehuray A. P. (1989b) Concentration, oxidation-state, and particulate flux of uranium in the Black Sea. *Geochim. Cosmochim. Acta* **53,** 2215–2224.

Anderson R. F., Lehuray A. P., Fleisher M. Q., and Murray J. W. (1989c) Uranium deposition in Saanich Inlet sediments, Vancouver Island. *Geochim. Cosmochim. Acta* **53,** 2205–2213.

Andersson P. S., Porcelli D., Gustafsson O., Ingri J., and Wasserburg G. J. (2001) The importance of colloids for the behavior of uranium isotopes in the low-salinity zone of a stable estuary. *Geochim. Cosmochim. Acta* **65,** 13–25.

Banner J. L., Wasserburg G. J., Chen J. H., and Moore C. H. (1990) ^{234}U-^{238}U-^{230}Th-^{232}Th systematics in saline groundwaters from central Missouri. *Earth Planet. Sci. Lett.* **101,** 296–312.

Barnes C. E. and Cochran J. K. (1990) Uranium removal in oceanic sedimentation and the oceanic balance. *Earth Planet. Sci. Lett.* **97,** 94–101.

Baskaran M., Santschi P. H., Guo L., Bianchi T. S., and Lambert C. (1996) ^{234}Th/^{238}U disequilibria in the Gulf of Mexico; the importance of organic matter and particle concentration. *Continental Shelf Res.* **16,** 353–380.

Baxter E. A. and DePaolo D. J. (2000) Field evidence for slow metamorphic reaction rates at 500–600°C. *Science* **288,** 1411–1414.

Berner R. A. (1980) *Early Diagenesis: A Theoretical Approach.* Princeton University Press.

Blum A. E., and Stillings L. L. (1995) Feldspar dissolution kinetics. In *Chemical Weathering Rates of Silicate Minerals*, Vol. 31, pp. 291–351. Mineralogical Society of America.

Blum J. D. and Erel Y. (1997) Rb-Sr isotope systematics of a granitic soil chronosequence: The importance of biotite weathering. *Geochim. Cosmochim. Acta* **61,** 3193–3204.

Bonotto D. M. and Andrews J. N. (1993) The mechanism of ^{234}U/^{238}U activity ratio enhancement in karstic limestone groundwater. *Chem. Geol.* **103,** 193–206.

Braithwaite A., Richardson S., Moyes L. N., Livens F. R., Bunker D. J., Hughes C. R., Smith J. T., and Hilton J. (2000). Sorption kinetics of uranium-238 and neptunium-237 on a glacial sediment. *Czech. J. Phys.* **50,** 265–269.

Brantley S. L., and Chen Y. (1995) Chemical weathering rates of pyroxenes and amphiboles. In *Chemical Weathering Rates of Silicate Minerals*, Vol. 31, pp. 119–172. Mineralogical Society of America.

Brantley S. L. and Mellott N. P. (2000) Surface area and porosity of primary silicate minerals. *Am. Miner.* **85,** 1767–1783.

Burch T. E., Nagy K. L., and Lasaga A. C. (1993) Free-energy dependence of albite dissolution kinetics at 80°C and Ph 8.8. *Chem. Geol.* **105,** 137–162.

Cama J., Ayora C., and Lasaga A. C. (1999) The deviation-from-equilibrium effect on dissolution rate and on apparent variations in activation energy. *Geochim. Cosmochim. Acta* **63,** 2481–2486.

Capo R. C. and DePaolo D. J. (1990) Seawater strontium isotopic variations from 2.5 million years ago to the present. *Science* **249,** 51–55.

Carter S. J. and Raymo M. E. (1999) Sedimentological and mineralogical control of multisensor track data at Sites 981 and 984. In *Proceedings of the Ocean Drilling Program, Scientific Results***162** (eds. M. E. Raymo, E. Jansen, P. Blum and T. D. Herbert), pp. 247–257. Ocean Drilling Program.

Channell J. E. T., and Lehman B. (1999) Magnetic stratigraphy of North Atlantic Sites 980–984. In *Proceedings ODP Scientific Results* (eds. M. E. Raymo, E. Jansen, P. Blum and T. D. Herbert). 162:College Station, TX. Ocean Drilling Project.

Chen J. H., Edwards R. L., and Wasserburg G. J. (1986) U-238, U-234 and Th-232 in Seawater. *Earth Planet. Sci. Lett.* **80,** 241–251.

Chen Y. and Brantley S. L. (1997) Temperature- and pH-dependence of albite dissolution rate at acid pH. *Chem. Geol.* **135,** 275–290.

Cheng H., Adkins J., Edwards R. L., and Boyle E. A. (2000) U-Th dating of deep-sea corals. **64,** 2401–2416.

Christensen J. N., Dresel E. P., Conrad M. E., Maher K., and DePaolo D. J. (2004) Identifying the sources of subsurface contamination at the Hanford site in Washington using high-precision uranium isotopic measurements. *Environ. Sci. Technol.* **38**, 3330–3337.

Cochran J. K. (1992) The oceanic chemistry of the uranium- and thorium-series nuclides. In *Uranium-Series Disequilibrium; Applications to Earth, Marine, and Environmental Sciences* (eds. M. Ivanovich and R. S. Harmon), pp. 334–395. Clarendon Press.

Cochran J. K., Carey A. E., Sholkovitz E. R., and Surprenant L. D. (1986) The geochemistry of uranium and thorium in coastal marine sediments and sediment pore waters. *Geochim. Cosmochim. Acta* **50,** 663–680.

Cochran J. K. and Krishnaswami S. (1980) Radium, thorium, uranium, and Pb-210 in deep-sea sediments and sediment pore waters from the north equatorial Pacific. *Am. J. Sci.* **280,** 849–889.

Colley S. and Thomson, J. (1992) Behavior and mobility of U series radionuclides in Madeira abyssal plain turbidites over the past 750,000 years. *Marine Geol.* **109,** 141–158.

Colley S., Thomson J., and Wilson T. R. S. (1984) Post-depositional migration of elements during diagenesis in brown clay turbidite sequences in the Northeast Atlantic. *Geochim. Cosmochim. Acta* **48,** 1223–1235.

Davis D. W. and Krogh T. E. (2001) Preferential dissolution of U-234 and radiogenic Pb from alpha-recoil-damaged lattice sites in zircon: Implications for thermal histories and Pb isotopic fractionation in the near surface environment. *Chem. Geol.* **172,** 41–58.

Davis J. A., Fuller C. C., and Cook A. D. (1987) A model for trace-metal sorption processes at the calcite surface: Adsorption of Cd-2+ and subsequent solid-solution formation. *Geochim. Cosmochim. Acta* **51,** 1477–1490.

Delaney M. L. and Boyle E. A. (1983) Uranium and thorium isotope concentrations in foraminiferal calcite. *Earth Planet. Sci. Lett.* **62,** 258–262.

Delanghe D., Bard E., and Hamelin B. (2002) New TIMS constraints on the uranium-238 and uranium-234 in seawaters from the main ocean basins and the Mediterranean Sea. *Marine Chemistry* **80,** 79–93.

DePaolo D. J. and Getty S. R. (1996) Models of isotopic exchange in reactive fluid–rock systems: Implications for geochronology in metamorphic rock. *Geochim. Cosmochim. Acta* **60,** 3933–3947.

DePaolo D. J. and Ingram B. L. (1985) High-resolution stratigraphy with strontium isotopes. *Science* **227,** 938–941.

Drever J. I. (1988) *The Geochemistry of Natural Waters.* Prentice-Hall.

Drever J. I. and Clow D. W. (1995) Weathering rates in catchments. In *Chemical Weathering Rates of Silicate Minerals*, Vol. **31** (eds. A. F. White and S. L. Brantley). Mineralogical Society of America.

Edwards R. L., Chen J. H., Ku T. L., and Wasserburg G. J. (1987) Precise timing of the last interglacial period from mass spectrometric determination of thorium-230 in corals. *Science* **236,** 1548–1553.

Eyal Y. and Fleischer R. L. (1985) Preferential leaching and the age of radiation-damage from alpha-decay in minerals. *Geochim. Cosmochim. Acta* **49,** 1155–1164.

Eyal Y. and Olander D. R. (1990a) Impact of alpha-decay on incongruent actinide isotope leaching from monazite. *J. Nucl. Mater.* **170,** 117–120.

Eyal Y. and Olander D. R. (1990b) Leaching of uranium and thorium from monazite. 1. Initial leaching. *Geochim. Cosmochim. Acta* **54,** 1867–1877.

Farley K. A., Wolf R. A., and Silver L. T. (1996) The effects of long alpha-stopping distances on (U-Th)/He ages. *Geochim. Cosmochim. Acta* **60,** 4223–4229.

Fleischer R. L. (1980) Isotopic disequilibrium of uranium: Alpha-recoil damage and preferential solution effects. *Science* **207,** 979–981.

Fleischer R. L. (1982a) Alpha-recoil damage and solution effects in minerals: Uranium isotopic disequilibrium and radon release. *Geochim. Cosmochim. Acta* **46,** 2191–2201.

Fleischer R. L. (1982b) Nature of alpha-recoil damage: Evidence from preferential solution effects. *Nuclear Tracks and Radiation Measurements* **6,** 35–42.

Fleischer R. L. (1983) Theory of alpha-recoil effects on radon release and isotopic disequilibrium. *Geochim. Cosmochim. Acta* **47,** 779–784.

Fleischer R. L. (1988) Nuclear track studies of alpha-recoil damage in nature: Relation to isotopic disequilibrium and leaching of radionuclides. *Nuclear Tracks and Radiation Measurements* **14,** 437–446.

Fleischer R. L. and Raabe O. G. (1978) Recoiling alpha-emitting nuclei: Mechanisms for uranium-series disequilibrium. *Geochim. Cosmochim. Acta* **42,** 973–978.

Fuhrmann M., Zhou H., Neiheisel J., Schoonen M. A. A., and Dyer R. (1997) Sorption/desorption of radioactive contaminants by sediment from the Kara sea. *Science of the Total Environment* **202,** 5–24.

Gariepy C., Ghaleb B., Hillaire-Marcel C., Mucci A., and Vallieres S. (1994) Early diagenetic processes in Labrador Sea sediments: Uranium-isotope geochemistry. *Can. J. Earth Sci.* **31,** 28–37.

Hamelin B., Bard E., Zindler A., and Fairbanks R. G. (1991) $^{234}U/^{238}U$ mass spectrometry of corals: How accurate is the U-Th age of the last interglacial period? *Earth Planet. Sci. Lett.* **106,** 169–180.

Henderson G. M., Martel D. J., Onions R. K., and Shackleton N. J. (1994) Evolution of seawater Sr-87/Sr-86 over the last 400-Ka: The absence of glacial interglacial cycles. *Earth Planet. Sci. Lett.* **128,** 643–651.

Henderson G. M., Slowey N. C., and Fleisher M. Q. (2001) U-. Th dating of carbonate platform and slope sediments. *Geochim. Cosmochim. Acta* **65,** 2757–2770.

Henderson G. M. Cohen, A. S., and O'Nions R. K. (1993) $^{234}U/^{238}U$ ratios and ^{230}Th ages for Hateruma Atoll corals: Implications for coral diagenesis and seawater $^{234}U/^{238}U$ ratios. *Earth Planet. Sci. Lett.* **115,** 65–73.

Hillaire-Marcel C., Aksu A., Causse C., de Vernal A., and Ghaleb B. (1990) Response of Th/U in deep Labrador Sea sediments (ODP Site 646) to changes in sedimentation rates and paleoproductivities. *Geology* **18,** 162–165.

Hochella M. F. and Banfield J. F. (1995) Chemical weathering of silicates in nature: A microscopic perspective with theoretical considerations. In *Chemical Weathering Rates of Silicate Minerals* Vol. 31, pp. 353–406.

Hodson M. E. (1998) Micropore surface area variation with grain size in unweathered alkali feldspars: Implications for surface roughness and dissolution studies. *Geochim. Cosmochim. Acta* **62,** 3429–3435.

Hodson M. E. and Langan S. J. (1999) The influence of soil age on calculated mineral weathering rates. *Appl. Geochem.* **14,** 387–394.

Hodson M. E., Langan S. J., Kennedy F. M., and Bain D. C. (1998a) Variation in soil surface area in a chronosequence of soils from Glen Feshie, Scotland and its implications for mineral weathering rate calculations. *Geoderma* **85,** 1–18.

Hodson M. E., Langan S. J., and Meriau S. (1998b) Determination of mineral surface area in relation to the calculation of weathering rates. *Geoderma* **83,** 35–54.

Hodson M. E., Lee M. R., and Parsons I. (1997) Origins of the surface roughness of unweathered alkali feldspar grains. *Geochim. Cosmochim. Acta* **61,** 3885–3896.

Hussain N. and Krishnaswami S. (1980) U-238 series radioactive disequilibrium in groundwaters: Implications to the origin of excess U-234 and fate of reactive pollutants. *Geochim. Cosmochim. Acta* **44,** 1287–1291.

Hussain N. and Lal D. (1986) Preferential solution of U-234 from recoil tracks and U-234/U-238 radioactive disequilibrium in natural-waters. *Proc. Ind. Acad. Sci.–Earth Planet. Sci.* **95,** 245–263.

Jeschke A. A. and Dreybrodt W. (2002) Dissolution rates of minerals and their relation to surface morphology. *Geochim. Cosmochim. Acta* **66,** 3055–3062.

Johnson T. M. and DePaolo D. J. (1997) Rapid exchange effects on isotope ratios in groundwater system. 1. Development of a transport-dissolution-exchange model. *Water Resources Res.* **33,** 187–195.

Johnson T. M., Roback R. C., McLing T. L., Bullen T. D., DePaolo D. J., Doughty C., Hunt R. J., Smith R. W., Cecil L. D., and Murrell M. T. (2000) Groundwater "fast paths" in the Snake River Plain aquifer: Radiogenic isotope ratios as natural groundwater tracers. *Geology* **28,** 871–874.

Kaufman M. I., Rydell H. S., and Osmond J. K. (1968) U234/U238 Disequilibrium as an aid to hydrologic study of Floridan aquifer. *Trans. Am. Geophys. Union* **49,** 165–178.

Kigoshi K. (1971) Alpha-recoil thorium-234: Dissolution into water and uranium-234/uranium-238 disequilibrium in nature. *Science* **173,** 47–49.

Kim K. (2002) Plagioclase weathering in the groundwater system of a sandy, silicate aquifer. *Hydrological Processes* **16,** 1793–1806.

Klinkhammer G. P. and Palmer M. R. (1991) Uranium in the oceans: Where it goes and why. *Geochim. Cosmochim. Acta* **55,** 1799–1806.

Knauss K. G. and Wolery T. J. (1986) Dependence of albite dissolution kinetics on Ph and time at 25°C and 70°C. *Geochim. Cosmochim. Acta* **50,** 2481–2497.

Kraemer T. F. and Kharaka Y. K. (1986) Uranium geochemistry in geopressured-geothermal aquifers of the United States Gulf-Coast. *Geochim. Cosmochim. Acta* **50,** 1233–1238.

Krane K. (1988) *Introductory Nuclear Physics*. Wiley.

Krishnaswami S., Graustein W. C., Turekian K. K., and Dowd J. F. (1982) Radium, thorium and radioactive lead isotopes in groundwaters: Application to the insitu determination of adsorption-desorption rate constants and retardation factors. *Water Resources Res.* **18,** 1663–1675.

Kronfeld J., Gradsztajn E., Muller H. W., Radin J., Yaniv A., and Zach R. (1975) Excess U-234: Aging effect in confined waters. *Earth Planet. Sci. Lett.* **27,** 342–345.

Ku T.-L., Luo S. D., Leslie B. W. and Hammond D. E. (1992) Decay-series disequilibria applied to the study of rock-water interaction and geothermal systems. In *Uranium-series Disequilibrium: Applications to Earth, Marine, and Environmental Science* (eds. M. Ivanovich and R. S. Harmon), pp. 630–671. Clarendon Press.

Ku T. L. (1965) An evaluation of U234/U238 method as a tool for dating pelagic sediments. *J. Geophys. Res.* **70,** 3457–3467.

Kump L. R., Brantley S. L., and Arthur M. A. (2000) Chemical, weathering, atmospheric CO_2, and climate. *Ann. Rev. Earth Planet. Sci.* **28,** 611–667.

Lasaga A. C. (1980) The kinetic treatment of geochemical cycles. *Geochim. Cosmochim. Acta* **44,** 815–828.

Lasaga A. C. (1998) *Kinetic Theory in the Earth Sciences.* Princeton University Press.

Lasaga A. C. and Berner R. A. (1998) Fundamental aspects of quantitative models for geochemical cycles. *Chem. Geol.* **145,** 161–175.

Lasaga A. C. and Luttge A. (2001) Variation of crystal dissolution rate based on a dissolution stepwave model. *Science* **291,** 2400–2404.

Lasaga A. C., Soler J. M., Ganor J., Burch T. E., and Nagy K. L. (1994) Chemical-weathering rate laws and global geochemical cycles. *Geochim. Cosmochim. Acta* **58,** 2361–2386.

Li Y. H. and Gregory S. (1974) Diffusion of ions in sea-water and in deep-sea sediments. *Geochim. Cosmochim. Acta* **38,** 703–714.

Luo S. D., Ku T. L., Roback R., Murrell M., and McLing T. L. (2000) In-situ radionuclide transport and preferential groundwater flows at INEEL (Idaho): Decay-series disequilibrium studies. *Geochim. Cosmochim. Acta* **64**, 867–881.

McKee B. A., Demaster D. J., and Nittrouer C. A. (1987) Uranium geochemistry on the Amazon Shelf: Evidence for uranium release from bottom sediments. **51**, 2779–2786.

Nagy K. L., Blum A. E., and Lasaga A. C. (1991) Dissolution and precipitation kinetics of kaolinite at 80°C and Ph 3: The dependence on solution saturation state. *Am. J. Sci.* **291,** 649–686.

Nagy K. L. and Lasaga A. C. (1992) Dissolution and precipitation kinetics of gibbsite at 80°C and Ph-3: The dependence on solution saturation state. *Geochim. Cosmochim. Acta* **56,** 3093–3111.

Raymo M. E., Jansen E., Blum P., and Herbert T. D. (1999) *Proceedings of the Ocean Drilling Project, Scientific Results.* Ocean Drilling Program.

Reynolds B. C., Wasserburg G. J., and Baskaran M. (2003) The transport of U- and Th-series nuclides in sandy confined aquifers. *Geochim. Cosmochim. Acta* **67,** 1955–1972.

Richter F. M. and DePaolo D. J. (1987) Numerical models for diagenesis and the neogene Sr isotopic evolution of seawater from Dsdp Site 590b. *Earth Planet. Sci. Lett.* **83,** 27–38.

Richter F. M. and DePaolo D. J. (1988) Diagenesis and Sr isotopic evolution of seawater using data from Dsdp-590b and Dsdp-575. *Earth Planet. Sci. Lett.* **90,** 382–394.

Richter F. M. and Liang Y. (1993) The rate and consequences of Sr diagenesis in deep-sea carbonates. *Earth Planet. Sci. Lett.* **117,** 553–565.

Roback R. C., Johnson T. M., McLing T. L., Murrell M. T., Luo S. D., and Ku T. L. (2001). Uranium isotopic evidence for groundwater chemical evolution and flow patterns in the eastern Snake River Plain aquifer, Idaho. *Geol. Soc. Am. Bull.* **113,** 1133–1141.

Rufe E. and Hochella M. F. (1999) Quantitative assessment of reactive surface area of phlogopite during acid dissolution. *Science* **285,** 874–876.

Russell A. D., Emerson S., Nelson B. K., Erez J., and Lea D. W. (1994) Uranium in foraminiferal calcite as a recorder of seawater uranium concentrations. *Geochim. Cosmochim. Acta* **58,** 671–681.

Santschi P. H., Bajo C., Mantovani M., Orciuolo D., Cranston R. E., and Bruno J. (1988) Uranium in pore waters from North-Atlantic (Gme and Southern Nares Abyssal-Plain) sediments. *Nature* **331,** 155–157.

Schrag D. P., Depaolo D. J., and Richter F. M. (1995) Reconstructing past sea-surface temperatures: Correcting for diagenesis of bulk marine carbonate. *Geochim. Cosmochim. Acta* **59,** 2265–2278.

Slowey N. C., Henderson G. M., and Curry W. B. (1996) Direct U-Th dating of marine sediments from the two most recent interglacial periods. *Nature* **383,** 242–244.

Stein M., Wasserburg G. J., Lajoie K. R., and Chen J. H. (1991) U-series ages of solitary corals from the California coast by mass-spectrometry. *Geochim. Cosmochim. Acta* **55,** 3709–3722.

Stewart B. W., Capo R. C., and Chadwick O. A. (2001) Effects of rainfall on weathering rate, base cation provenance, and Sr isotope composition of Hawaiian soils. *Geochim. Cosmochim. Acta* **65,** 1087–1099.

Taylor A. and Blum J. D. (1995) Relation between soil age and silicate weathering rates determined from the chemical evolution of a glacial chronosequence. *Geology* **23,** 979–982.

Taylor A. S., Blum J. D., and Lasaga A. C. (2000) The dependence of labradorite dissolution and Sr isotope release rates on solution saturation state. *Geochim. Cosmochim. Acta* **64,** 2389–2400.

Tessier A., Campbell P. G. C., and Bisson M. (1979) Sequential extraction procedure for the speciation of particulate trace-metals. *Anal. Chem.* **51,** 844–851.

Thomson J., Wallace H. E., Colley S., and Toole J. (1990) Authigenic uranium in Atlantic sediments of the last glacial stage: A diagenetic phenomenon. *Earth Planet. Sci. Lett.* **98,** 222–232.

Tricca A., Porcelli D., and Wasserburg G. J. (2000) Factors controlling the groundwater transport of U, Th, Ra, and Rn. *Proc. Ind. Acad. Sci.–Earth Planet. Sci.* **109,** 95–108.

Tricca A., Wasserburg G. J., Porcelli D., and Baskaran M. (2001) The transport of U- and Th-series nuclides in a sandy unconfined aquifer. *Geochim. Cosmochim. Acta* **65,** 1187–1210.

White A. F. (1995) Chemical weathering rates of silicate minerals in soils. In *Chemical Weathering Rates of Silicate Minerals*, Vol. 31, pp. 407–461. Mineralogical Society of America.

White A. F. and Blum A. E. (1995) Effects of climate on chemical-weathering in watersheds. *Geochim. Cosmochim. Acta* **59,** 1729–1747.

White A. F., Blum A. E., Schulz M. S., Bullen T. D., Harden J. W., and Peterson M. L. (1996) Chemical weathering rates of a soil chronosequence on granitic alluvium. 1. Quantification of mineralogical and surface area changes and calculation of primary silicate reaction rates. *Geochim. Cosmochim. Acta* **60,** 2533–2550.

White A. F., Blum A. E., Schulz M. S., Vivit D. V., Stonestrom D. A., Larsen M., Murphy S. F., and Eberl D. (1998) Chemical weathering in a tropical watershed, Luquillo mountains, Puerto Rico: I. Long-term versus short-term weathering fluxes. *Geochim. Cosmochim. Acta* **62,** 209–226.

White A. F, Brantley S. L (1995) Chemical weathering rates of silicate minerals: An overview. In *Chemical Weathering Rates of Silicate Minerals* Vol. 31, pp. 1–22.

White A. F. and Brantley S. L. (2003) The effect of time on the weathering of silicate minerals: Why do weathering rates differ in the laboratory and field? *Chem. Geol.* **202,** 479–506.

White A. F., Bullen T. D., Schulz M. S., Blum A. E., Huntington T. G., and Peters N. E. (2001) Differential rates of feldspar weathering in granitic regoliths. *Geochim. Cosmochim. Acta* **65,** 847–869.

Wood B. J. and Walther J. V. (1983) Rates of hydrothermal reactions. *Science* **222,** 413–415.

Wood B. J. and Walther J. V. (1986) Fluid flow during metamorphism and its implications for fluid–rock ratios. In *Fluid–Rock Interactions during Metamorphism*, Vol. **5** (eds. J. V. Walther and B. J. Wood), pp. 89–108. Springer-Verlag.

Wright A. K. and Flower B. P. (2002) Surface and deep ocean circulation in the subpolar North Atlantic during the mid-Pleistocene revolution. *Paleoceanography* **17**, 1068–1084.

Yamada M. and Tsunogai S. (1984) Postdepositional enrichment of uranium in sediment from the Bering Sea. *Marine Geol.* **54,** 263–276.

Yokoyama Y. and Nguyen H (1980) Direct and non-destructive dating of marine sediments, manganese nodules, and corals by high-resolution gamma-ray spectrometry. In *Isotope Marine Chemsitry* (eds. E. D. Goldberg, Y. Horibe, and K. Saruhashi), pp. 259–289. Uchida Rokakudo Publishing Co., Tokyo.

You C. F., Chan L. H., Gieskes J. M., and Klinkhammer G. P. (2003) Seawater intrusion through the oceanic crust and carbonate sediment in the Equatorial Pacific: Lithium abundance and isotopic evidence. *Geophys. Res. Lett.* **30**.

Zheng Y., Anderson R. F., Van Geen A., and Fleisher M. Q. (2002a) Preservation of particulate non-lithogenic uranium in marine sediments. *Geochim. Cosmochim. Acta* **66,** 3085–3092.

Zheng Y., Anderson R. F., Van Geen A., and Fleisher M. Q. (2002b) Remobilization of authigenic uranium in marine sediments by bioturbation. *Geochim. Cosmochim. Acta* **66,** 1759–1772.